Yield Calculations for production of medically important ^{64}Cu and ^{68}Ga radionuclides produced in α + ^{66}Zn reaction at ≈ 10 - 40 MeV

A Thesis Submitted to School of Graduate Studies College of Natural and Computational Science in Partial Fulfillment of the Requirements for the Degree of Master of Science in Physics.

By

Tekalegn Mitiku

Hawassa, Ethiopia

May, 2024

Declaration

I hereby declare that this MSc thesis is my original work and has not been presented for a degree in any other university, and that all sources of material used for the thesis have been duly acknowledged.

Name: Tekalegn Mitiku
Signature:
Email: tekalignmitiku1335@gmail.com

This MSc thesis has been submitted for examination with my approval as university advisor.

Name:-
Amanuel Fessahatsion (PhD) Signature: _____

Place and date of submission:

Hawassa, Ethiopia
May, 202

Hawassa University

Schools of Graduate Studies

Examiner's Approval Sheet

We, the undersigned, members of the broad of examiners of the final open defense by Tekalign Mitiku Daimo have read and evaluated his thesis in entitled "**Yield calculation for production of medically important ^{64}Cu and ^{68}Ga radionuclide produced in α + ^{66}Zn reaction at ≈10-40 MeV"** and examined the candidate. This is therefore to certify that the thesis has been accepted in partial fulfillment of the requirement for the degree of Masters in Physics.

Name of Major Advisor	Signature	Date
Name of Internal Examiner- I	Signature	Date
Name of Internal Examiner -II	Signature	Date
Name of External Examiner	Signature	Date
SGS Approval	Signature	Date

Finally approval and acceptance of the thesis is contingent up on the submission of the finally copy of the thesis to the school of Graduate studies (SGS) through the Department/School graduate committee (DGC/SGS) of the candidate's department.

Stamp of SGS Date: _____

Hawassa University

College of Natural and Computational Sciences

Department of Physics

Advisor Approval sheet

The undersigned hereby certify that they have read and recommend to the College of Natural and computational Science School of Graduate Studies for acceptance MSc Thesis entitled "**Yield calculation for production of medically important ^{64}Cu and ^{68}Ga radionuclide produced in α + ^{66}Zn reaction at ≈10-40 MeV''** by author Tekalign Mitiku Daimo in partial fulfillment of the requirements for the degree of Masters in Physics.

Approved by:

Name of Advisor	Signature	Date
_____	_____	_____
Department Head	Signature	Date
_____	_____	_____

ACKNOWLEDGEMENT

I would like to extend my sincere gratitude to all those who contributed to the successful completion of this study. Firstly, I would like to thank my research advisor, Dr. Amanuel Fessahatsion, for his invaluable guidance, continuous support, and insightful feedback throughout this research. His expertise and encouragement have been instrumental in the development and completion of this work. I am grateful to all my family members, especially to my sister Fanaye Mitiku and my brother Hosiana Memire (Babi) for their unwavering support, patience, and understanding throughout the duration of this work. I am also thankful to Tiguaded Yeneabat and Yegnanesh Fenta, physics lecturers at Hawasa University, for their technical assistance and continuous support. Lastly, I would like to express my deepest gratitude to Gena Woreda Administration Office for giving me this opportunity to attend the masters program.

Thank you all for your contributions and support.

ABSTRACT

This work studied the production cross section and yield of medically important radionuclides, such as ^{68}Ga and ^{64}Cu, generated during irradiation of ^{66}Zn-target with α-projectile at ≈ 10-40

MeV. The experimental cross-sections taken from the EXFOR database were compared with the theoretical model calculations using nuclear reaction model codes COMPLETE, TALYS1.95 (G), and EMPIRE3.2. A good agreement was achieved for the measured data and calculated production cross-section using the TALYS1.95 (G) code. The ^{68}Ga and ^{64}Cu yields were computed using TALYS1.95 (G) predicted cross-section data. Also, the possible isotopic impurities were identified, and their contributions were estimated. Based on the yield calculations, the production yield of ^{68}Ga was found to be 39.6 GBq/μAh, at 28 MeV without any significant contribution from its isotopic impurities ^{67}Ga and ^{66}Ga; in addition a yield value of 85.9 MBq/μAh at 40 MeV was obtained for medically important ^{64}Cu radionuclide with negligible isotopic impurities contributions from ^{66}Cu and ^{62}Cu radionuclides.

Table of Contenrts

ACKNOWLEDGEMENT iv
ABSTRACT iv
LIST OF ABBREVATIONS viii
LIST OF FIGURES ix

LIST OF TABLES x
CHAPTER ONE 1
INTRODUCTION 1
1.1. Objectives of the study 4
1.1.1. General Objective 4
1.1.2. Specific Objectives 4
1.2. Significance of the study 4
CHAPTER TWO 5
THEORETICAL BACKGROUND 5
2.1. Description of nuclear reaction 5
2.2. Classifications of Nuclear reaction 7
2.2.1. Direct reaction 7
2.2.2. Pre-equilibrium reactions and models 7
2.2.2.1. Exciton Model (EM) 8
2.2.2.2 Geometry Dependent Hybrid Model (GDH) 9
2.2.3. Compound nuclear reaction and models 10
2.2.3.1. Fermi-Gas Model 14
2.2.3.2. Generalized Super Fluid Model 15
2.2.3.3. Enhanced Generalized Super Fluid Model 16
2.2.3.4. Optical Model (OM) 17
2.4. Nuclear reaction cross section 19
2.4.1. Partial wave analysis of reaction cross-section 20
2.5. Thick target yield 25
CHAPTER THREE 28
COMPUTER CODE AND FORMULATIONS 28
3.1 COMPLETE code 28
3. 2. TALYS1.95 (G) 29
3.3. EMPIRE3.2 30
3.4. Weiss Kopf-Ewing Formulation 30
3.5. Hauser-Feshbach Formulation 33
3.6. Pearson's correlation coefficient 34
3.7. Thick Target Yield calculations 36
CHAPTER FOUR 37

RESULT AND DISCUSSIONS 37
4.1. Production of ^{68}Ga Radionuclide 39
4.1.1. Contribution of isotopic impurities in ^{68}Ga production 40
4.2. Production of ^{64}Cu Radionuclide 42
4.2.1. Contribution of isotopic impurities in ^{64}Cu production 44
4.3. Thick target yield 45
4.3.1. Thick target yields of ^{68}Ga and its isotopic impurities ^{67}Ga, ^{66}Ga 45
4.3.2. Thick target yields of ^{64}Cu and its isotopic impurities ^{66}Cu, ^{62}Cu 47
CHAPTER FIVE 49
SUMMARY AND CONCLUSION 49
REFERENCES 50

LIST OF ABBREVATIONS

PET Positron Emitting Tomography

HMB Harp Miller Berne

PSMA Prostate-Specific Membrane Antigen

INC Inter Nuclear Cascade

EM Exciton model

GDH Geometry dependent hybrid

CN Compound nucleus

PE Pre-equilibrium

IAEA International Atomic Energy Agency

OMP Optical Model Parameter

TTY Thick Target Yield

NRDC International Network of Nuclear Reaction Data Centers

MFM Mean Free Path Multiplier

GSFM Generalized Super Fluid Model

EGSFM Enhanced Generalized Super Fluid Model

EOB End -Of-Bombardment

LIST OF FIGURES

Figure 2.1. Representation of the equilibration process as formulated in the exciton model [19]. 9
Figure 2.2. Schematic drawing of nuclear reaction [28]..... 13
Figure 2.3. Possible values of scattering and reaction cross-section. 25
Figure 4.1. Experimentally measured and theoretically predicted cross sections of ^{68}Ga..... 38
Figure 4.2. Experimentally measured and theoretically predicted cross section of ^{68}Ga. 40
Figure 4.3. Calculated cross sections of radionuclide impurities of gallium produced in alpha-induced reaction on ^{66}Zn using TALYS 1.95(G)..... 42
Figure 4.4. Experimentally measured and theoretically predicted excitation functions of ^{64}Cu.. 43
Figure 4.5.Calculated cross sections of radionuclide impurities of copper produced in alpha-induced reaction on ^{66}Zn using TALYS 1.95(G)..... 44
Figure.4.6.Calculated thick target yields for the ^{66}Zn(α,x)^{68}Ga, ^{66}Zn(α,x)^{67}Ga and ^{66}Zn(α,x)^{66}Ga reactions. 46
Figure.4.7.Calculated thick target yields for the ^{66}Zn(α,x)^{64}Cu, ^{66}Zn(α,x)^{66}Cu and ^{66}Zn(α,x)^{62}Cu reactions. 47

LIST OF TABLES

Table 1: Q values and threshold energies for investigated ^{68}Ga, ^{67}Ga, and ^{66}Ga radionuclides ... 41

Table 2: Pearson's correlation coefficient, R, between experimental measured and theoretical predicted values of Levkovski [48] and Nagame [52]. ... 43

Table 3: Investigated nuclear reactions for the production of ^{64}Cu, ^{66}Cu, and ^{62}Cu with their Q values and threshold energies. ... 44

Table 4: Comparison of ^{68}Ga yields and predicted radioactive impurity yields for some selected alpha energies ... 46

Table 5: Comparison of ^{64}Cu yields and predicted radioactive impurity yields for some selected alpha energies ... 48

CHAPTER ONE

INTRODUCTION

The history of nuclear reaction investigations begins in 1909–1911 when Rutherford's team observed large-angle elastic scattering of alpha particles by thin foils of the metals and discovered the nuclei of Au and Pt atoms [1]. However, Fermi et al. conducted the first systematic investigations of nuclear reaction mechanisms from 1932 to 1933 [2]. They used the newly discovered neutrons to irradiate 38 nuclides, ranging from hydrogen to uranium, and then they observed the resulting radioactivity. A nuclear reaction is a process by which two nuclear particles (two nuclei or a nucleus and a nucleon) interact to produce two or more nuclear particles or gamma rays. The incoming nuclei and the outgoing reaction products during the interaction indicate an energy and momentum exchange [3]. This process occurs when radioactive materials or particles from an accelerator bombard a target.

The cross-section data of nuclear reactions is the quantitative feature of nuclear reactions that can reveal details about the characteristics of excited nuclear states and various reaction mechanisms. The development of new ideas for the generation of nuclear energy, the conversion of radioactive waste, the building of accelerator shields, nuclear reactors, the production of medical isotopes, and numerous other related applications all require access to nuclear data. These nuclear data are critical to producing radionuclides, particularly for medically useful radionuclides [4]. Artificially produced radionuclides have several uses in business, agriculture, medicine, and nuclear research [5]. Typical uses of these medically important radionuclides include therapy, diagnosis, and research [6]. Nuclear reaction data are mainly required for optimization of production routes in radioisotope production programs [7]. Separating the radioisotope from the target material is essential for producing radioisotopes in the nuclear reaction. Even with the highest isotopic enrichment and the most exact energy selection, it is only sometimes possible to completely remove the radioactive impurities. Understanding reaction cross-sections is essential to solving this issue. The energy value at the maximum cross-sectional energy of radioisotope production, where the cross-sectional data for the other reaction pathways are minimum, should be used to determine the beam energy [8].

In the past, theoretical calculations on the production cross–section and yield of radioisotopes have an undeniable importance for the investigation of new production routes.

Artun [9] investigated the production of ^{201}Pb, ^{198}Au, ^{186}Re, ^{111}Ag, ^{103}Pd, ^{90}Y, ^{89}Sr, ^{77}Kr, ^{77}As, ^{67}Cu, ^{64}Cu, ^{47}Sc, and ^{32}P therapeutic radioisotopes from various projectile-target systems by the reaction of ^{48}Ti(p, 2p)^{47}Sc, ^{32}S(n, p)^{32}P, ^{64}Ni(d, 2n)^{64}Cu ^{64}Ni(p, n)^{64}Cu, ^{64}Zn(n, p)^{64}Cu, ^{68}Zn(p,2n)^{67}Cu, ^{70}Zn(p, α)^{67}Cu, ^{80}Se(p, α)^{77}As, ^{79}Br(p, 3n)^{77}Kr, ^{89}Y(n, p)^{89}Sr, ^{90}Zr(n, p)^{90}Y, ^{110}Pd(d, n)^{111}Ag, ^{186}W(p, n)^{186}Re, and ^{198}Pt(p, n)^{198}Au. Theoretical predictions of cross-sections were done using the TALYS and EMPIRE codes for different level density models. The obtained results showed that the model results with the TALYS and EMPIRE codes were consistent with the experimental data for many reactions; however, the results with the TALYS code are generally a little bit more consistent than that of the results with the EMPIRE code, especially the integral yield results. The integral yield results indicated that the curves of ^{64}Ni(d, 2n)^{64}Cu, ^{64}Ni(p, n)^{64}Cu, ^{68}Zn(p,2p)^{67}Cu, ^{110}Pd(d, n)^{111}Ag and ^{186}W(p, n)^{186}Re reactions are close to the experimental data. Moreover the model result of ^{103}Rh(d, 2n)^{103}Pd, ^{186}W(d,2n)^{186}Re, and ^{203}Tl(p,3n)^{201}Pb reactions overlap with the experimental data and the recommended data. Additionally, it has been noted that the amount of the integral yield results of reactions for the production of the cancer therapy radioisotopes is restricted in the literature based on both the experimental data and theoretical results.

Aslam et al. [10] studied the production ^{68}Ga via α-particle induced reactions on enriched copper, ^{65}Cu target up to 40 MeV. The available data sets of experimental cross-sections taken from the IAEA database were compiled, normalized, and compared with the theoretical model calculations using nuclear reaction model codes ALICE-IPPE, TALYS 1.95, and EMPIRE3.2. The study indicated good agreement between the normalized measured cross-section data and the theoretically calculated. A thick target yield of 732MBq/μAh was obtained from the recommended cross-sections of ^{65}Cu(α,n)^{68}Ga reaction. Further, the study investigated the possible radio-impurities that could be contributed using the reaction model code TALYS1.95. Based on the yield analyses, the study concluded that ^{65}Cu(α, n)^{68}Ga reaction is a potential route for the production of ^{68}Ga at low-energy cyclotrons due to negligible radio-impurities in the region of 7 MeV→14 MeV.

Kambali et al. [11] investigated the Optimum radioactivity yield of ^{89}Zr radionuclide produced by bombarding ^{89}Y-target with variable proton energies ranging from 11 to 30 MeV. The production yield and its radioactive impurities present during ^{89}Zr production were calculated. The results indicated that the radioactivity yield of ^{89}Zr produced by 11 MeV proton was 41.18MBq/μAh, whereas the yield increased significantly to 166.76MBq/μAh when the ^{89}Y-target was bombarded with 30MeV protons. The higher ^{89}Zr radioactivity yields also resulted in higher radioactive impurities, which could be of concern when applied to patients. By assuming that the radioactive impurities came from proton interactions with the ^{89}Y- target, it was found that the 11 and 13 MeV proton-bombarded ^{89}Y-targets resulted in no radioactivity impurities. The radioactive impurities became significantly high when more significant than 18 MeV protons were employed.

Recently, Amjed et al. [12] evaluated cross-section data for production of the ^{90}Nb radionuclide by the reaction of ^{90}Zr(p, n)^{90}Nb, ^{91}Zr(p, 2n)^{90}Nb, ^{90}Zr(d, 2n)^{90}Nb, ^{90}Y(α, 3n)^{90}Nb and ^{93}Nb(p, 4n)^{90}Mo→^{90}Nb. For each production route, the reliability and consistency of the experimental data were critically analyzed on the basis of three nuclear model calculations, namely, TALYS 1.9, ALICE-IPPE, and EMPIRE 3.2. A well-developed methodology was used to calculate the recommended data for each excitation function based on the experimental data and the results of theoretical nuclear models. The same was done for reactions leading to possible radioisotopic impurities. Thick target yields were calculated using the recommended data for each production route and its corresponding impurity reactions. Numerical values of integral yields in the suggested energy region with the percentage level of contributing radioisotopic impurities were given. It was found that the ^{90}Zr(p,n)^{90}Nb production route is better served for low energy cyclotrons (20→5MeV) production, and the ^{91}Zr(p,2n)^{90}Nb and ^{90}Zr (d,2n)^{90}Nb production routes are suitable for medium energy cyclotron (30→12 MeV) production. Furthermore ^{93}Nb(p, 4n)^{90}Mo→^{90}Nb and ^{89}Y(α,3n)^{90}Nb production route are suitable for high energy cyclotron(80→31MeV) production.

Practical calculations in terms of cross sections and the thick target yield of alpha-induced radioisotope are undeniable in investigating optimized new production routes. Despite the immense importance of medically important radionuclides produced in α-induced reactions, reasonable production yield studies for medically important radionuclides produced in α-induced reactions have not been investigated efficiently and still need further investigations.

In this work, the production yields of medically important ^{64}Cu and ^{68}Ga radionuclides produced in α + ^{66}Zn system from ≈ 10 - 40 MeV α-energies were studied. ^{64}Cu ($T_{1/2}$ = 12.7 h) is a unique radionuclide that can decay in all three ways, which makes it a powerful tracer for Positron Emitting Tomography (PET) and radiotherapy applications. ^{68}Ga radionuclide ($T_{1/2}$ = 67.71 min) becomes the first widespread generator-produced positron emitter in PET imaging. First introduced for the imaging of neuroendocrine tumors (^{68}Ga-labeled-DOTA-TOC), more recent significant success has been achieved for prostate cancer diagnosis and staging (^{68}Ga-DOTA-PSMA and derivatives) [13]. Theoretical predictions were carried out using the statistical model codes COMPLETE, EMPIRE3.2, and TALYS1.95 (G).

1.1. Objectives of the study

1.1.1. General Objective

- To calculate the production yields of medically important ^{64}Cu and ^{68}Ga radionuclides produced in α + ^{66}Zn system at ≈ 10-40 MeV.

1.1.2. Specific Objectives

- To optimize the theoretical model codes input parameters to produce the measured data.
- To identify the respective isotopic impurities and evaluate their contributions.
- To find the projectile energy point that produced the optimized production cross-section.

1.2. Significance of the study

Studying the production yields of the medically important radioisotopes produced in α-induced reactions on ^{66}Zn-target isotopes can provide valuable insights into optimized production routes and production energies, which can further serve as inputs for advanced research in nuclear medicine and practical applications of the radiopharmaceutical in advancing medical imaging and nuclear therapy (targeted cancer treatments). Further, the present work is used as a reference for other researcher and learners to develop the experience of using theoretical nuclear reaction codes and EXFOR database.

CHAPTER TWO

THEORETICAL BACKGROUND

2.1. Description of nuclear reaction

A nuclear reaction is a process by which the nucleus and the bombarding particle are in close proximity to one another (within a distance of approximately (10^{-15} m) [14]. A nuclear reaction occurs when a nucleon or combination of nucleons, or heavy ions, come into close contact with another nucleon or combination of nucleons. It is a process where a target nucleus is bombarded with gamma rays or nuclear probes to create a new system with either new energy or new composition, or both. Quantum numbers of energy levels, transition rates between levels, and the energies of binding and excitation can all be measured via reactions that exchange energy or nucleons. Nuclear reaction can be initiated by any types of projectiles neutron, proton, deuteron, and alpha particles and other nuclei positively charged, and so required enough energy to overcome the coulomb barrier. Elastic or inelastic scattering may occur when a projectile's proton, deuteron, and alpha particles approach and interact with the target nucleus.

Nuclear reactions are main approach for examining the structure of complex nuclei, the nature of the nuclear force, and the process for creating radioactive nuclei for research or applications [15]. Depending on the kinetic energy of the accelerating nucleus, several interactions between the two approaching nuclei are possible. These interactions fall into two categories: nuclear reactions and scattering mechanisms. Target and projectile nuclei are the two general categories for the interacting nuclei. If the kinetic energy of the projectile is too low to penetrate the target nucleus, it will be scattered elastically or in-elastically, thereby transferring excitation energy to the target nucleus in the latter case. A nuclear reaction that changes the target nucleus's atomic and/or mass number may actually occur if the interacting nucleus' energy is high enough to penetrate the target nucleus [16]. Nuclear reactions can be written down in a manner similar to chemical reaction equations. If a target nucleus X is bombarding by particle x, during this process a new nucleus Y is formed and particle y is emitted.

Generally nuclear reaction can be expressed;

$$x + X \rightarrow Y + y + Q \qquad (2.1)$$

Where 'x' is energetic bombarding particles (projectiles)

'X' is the target particles which was initially at rest

'Y' is the new nuclei is called residual nucleus.

'y' is the emitted (outgoing) particles.

'Q' is the energy released during the reaction, so that Q is positive for exoergic reaction and 'Q'is negative for endoergic reaction.

In compact form it can be written as, X (x, y) Y.

If more than one particle say y_1, y_2 and y_3 are emitted then the reaction is written as [14]

$$x + X \rightarrow Y + y_1 + y_2 + y_3 + Q \qquad (2.2)$$

It denoted as X (x; y_1 y_2 y_3) Y

Where: x = the bombarding particle (projectile),

X = target nucleus

Y = Residual nucleus

y = outgoing particle

Q = the energy released in the reaction given by

$$Q = (M_a + M_x)C^2 - \left(M_y + M_b\right)C^2 \qquad (2.3)$$

In which

M_a = mass of the projectile

M_x = mass of the target nucleus,

M_y= mass of the residual nucleus,

M_b = mass of the released particle (ejectile)

C = the speed of light

In nuclear reactions, the projectile can be proton, neutron, deuteron, alpha particle, etc., and /or any other heavy ions. The emitted particles may be a nucleon, a nucleus or gamma radiations.

Nuclear reactions are generally understood to be reactions in which particles interact with nuclides to produce both particles and nuclides [17]. The nucleons in the incident particle or projectile must interact with the nucleons in the target in order for a nuclear reaction to take place. Therefore, the energy needs to be high enough to overcome the protons' inherent electromagnetic repulsion.

2.2. Classifications of Nuclear reaction

Depending on the mechanism through which the reaction takes place; nuclear reaction can be subdivided into three categories (i) direct reaction. (ii). Compounds reaction. (iii) Pre -equilibrium reaction. The contribution of this process depends on the given reaction and the energy of the incident particles. The three types can be distinguished by their angular distribution and the time scales**.**

2.2.1. Direct reaction

Direct reaction is an extremes side of the compound reaction. A direct reaction is one that happens without a compound nucleus starting to form. It is therefore a one-step process [18]. Direct reactions occur when a projectile particle interacts with a very small number of nucleons on the target nucleus' surface without the creation of an intermediate compound system; these reactions are referred to as peripheral processes. This reaction happens straight from the entrance to an exit channel, without the creation of an intermediate state. A direct reaction takes place when the projectile primarily interacts with the nucleons on the target nucleus' surface. One or two nucleons are involved in the interaction. Only a few nucleons receive energy and momentum transfer, and the particle's emission is most likely directed in the projectile's direction of motion. As the energy of the incident particle increases, its de Broglie wavelength decreases, making it more likely to interact with a nucleon-sized object rather than atomic-sized object [19]. It is most likely that a direct reaction process will occur on a target nucleus's surface without affecting the internal degrees of freedom in the remaining nucleus.

2.2.2. Pre-equilibrium reactions and models

Direct reaction and compound-nucleus are the limiting cases; however it is not possible to define a separation line between these two processes.

There are intermediate-type nuclear reactions. Before equilibrium is attained, a compound system made up of the target nucleus and an incident particle may disintegrate; in this case, the emission is called a pre-compound emission. It can happen that a particle is neither emitted immediately after the interaction as in the direct reaction case nor after long time by statically decay of the compound nucleus. The projectiles may share its energy among a small number of nucleon which may further interact with other nucleon and during this cascade of nucleon-nucleon interaction through which the projectiles energy is progressively shared among the target nucleons a particle may be emitted along before the attainment of statistical equilibrium. These processes are referred to as pre-equilibrium reaction. Pre-equilibrium reaction is defined as a reaction mechanism in which the target nucleus undergoes disintegration before compound nucleus or equilibrium is reached. The particles are emitted after the first stage of a direct reaction but long before the attainment of compound nucleus formation [20].

These reactions are typically multi-step processes within a quantum mechanical framework. It is imagined that the incident particle step-by-step creates more complex states of the compound system and gradually loses its memory of the initial energy and direction. The evaluation of nuclear data is typically done using experimental data and theoretical model calculations. For a wide range of energies, measuring the required cross-sections for every isotope in the periodic table is not possible economically or practically. In many cases, nuclear reaction models are required to provide estimates of the particle-induced reaction cross-sections; this is particularly the case when experimental data are unavailable or when the cross-sections are too difficult to measure. Consequently, the evaluation of nuclear data greatly benefits from the computation of nuclear reaction models [21]. The pre-equilibrium models became a rather popular tool to analyze and understand nuclear reactions at excitation energies ranging from several tens of MeV up to the GeV regions. It includes the exciton model and the geometry dependent hybrid (GDH) model.

2.2.2.1. Exciton Model (EM)

Exciton model is presented by Griffin and is logically simple and modified. According to this model, an initial configuration composed of a few excitons, excited particles and holes is formed when the incoming projectile interacts with the target nucleus [14]. The exciton number, or the total number of particles (p) above and holes (h) below the Fermi surface and the excitation energy of the composite nucleus define the nuclear state.

Excitons rise with successive two-body interactions, resulting in a residual nucleus that is fully equilibrated. Griffin proposed two fundamental theories to explain each phase of the composite nucleus.

1. Every state in the cascade is equiprobable at every point where all of the states have the same configurations and total energy.
2. Every possible process at every stage of the cascade is equiprobable [22].

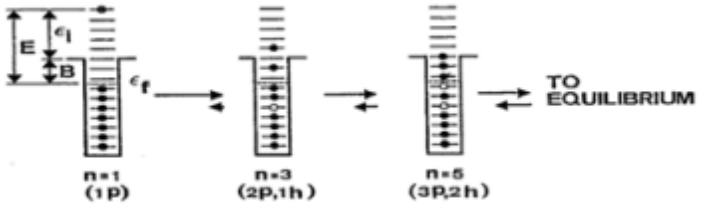

Figure.2.1. Representation of the equilibration process as formulated in the exciton model [19].

The symbols as indicated in figure 2.1 represent:

E = Excitation energy B = binding energy

- = particle n = number of exciton
- = hole ε_f = Fermi energy

Since all the levels below the Fermi energy are filled, the first projectile-target interaction brings two particle-one hole (2p+ 1h) state which produces a total exciton number of 3;

i.e. $n = p + h = 3$, the next interaction may be (3p, 2h) state, i.e. $n = p + h = 5$ and so on. In this cascade interactions, $\Delta p = 0, \pm 1$ and $\Delta h = 0, \pm 1$; then $\Delta n = 0, \pm 2$.

The pre-equilibrium exciton model is governed by the set of master equation which describes both competing processes the equilibrium of the nucleus and the emission. In the simple case, when we consider just one possible excitation energy and only the composite system prior to and including the first emission, this set reads [14].

2.2.2.2 Geometry Dependent Hybrid Model (GDH)

In a geometry-dependent hybrid model the pre-equilibrium decay can be influenced by the target nucleus's nucleon density distribution. The HMB and exciton model combinations are described by this model. It makes the assumption of a lower matter density and takes geometry effects into account.

The model takes into account both equilibrium decay and multi-pre-equilibrium particle emission. It computes the emission spectra of the projectile-target nucleus interaction at each stage of the energy dissipation process [23]. A popular hybrid H model for explaining the pre-compound (PC) reaction mechanism was initially proposed by Blann [24]. According to Blann, the following formula can be used to determine the PC differential reaction cross section:

$$\frac{d\sigma_v}{d\epsilon} = \sigma_R p_v(\varepsilon) \qquad (2.4)$$

Here, σ_R represents the reaction cross section, and the term $p_v(\varepsilon)$ represents the number of particles of the type emitted into the unbounded continuum with channel energy between ε and $\varepsilon + d\varepsilon$. The geometry-dependent hybrid (GDH) model has been able to reasonably reproduce a wide range of data for many years [25]. The GDH model is a refined and modified version of the H model that takes into account the effects of nuclear geometry and lower matter density, thereby maintaining a shallow potential. Thus, the GDH model's PC emission formalism was extended to include the diffused surface properties of higher impact parameters. Thus, in the GDH model, the differential reaction cross section for PC emission is expressed as follows:

$$\frac{d\sigma_v(\varepsilon)}{d\varepsilon} = \pi\lambda^2 \Sigma_{l=0}^{\infty}(2l+1)T_l P_v(l,\varepsilon) \qquad (2.5)$$

T_l represents the transmission coefficient for the l^{th} partial wave, and the quantity $p_v(l,\varepsilon)$ represents decay probability at 'ε' channel energy and 'l' orbital angular momentum. 'λ' is the reduced de-Broglie wavelength.

2.2.3. Compound nuclear reaction and models

The compound nuclear reaction model was proposed first by Bohr in 1936. Compound nucleus reactions occur when a projectile collides with a target nucleus and the two combine to form a new nucleus (CN). According to Niles Bohr (1936), nuclear reaction of a certain type undergoes in two stages, the capture of incident particle (projectile) by the target nucleus to form a compound nucleus and the decay of the compound nucleus. Thus a nuclear reaction is described by;

$$x + X \rightarrow C^* \rightarrow Y + y \qquad (2.6)$$

Where C* is a compound system in excited state. This process takes so much time, that the system C* formed forgets the history of its formation. i.e., C* does not know what was the projectile x and what was the target Y.

The compound nucleus reaction can be treated as a two-step process. The first steps the incident particles stays in the nucleus for a relatively long time (10^{-16}sec) compared with the time that would be required for a particles to travel across the nucleus forming a compound nucleus and giving its energy to many nucleon in the target nucleus, This indicates that the compound nucleus forgets its history of formation by the time it decays. That is to say, the compound nucleus's decay is independent of its specific creation mode and only dependent on its energy (Ec), angular momentum, and parity. In the second step the compound nucleus disintegrate (decay) by ejecting a particle (proton, deuteron, and alpha particles) or gamma ray leaving the final or product nucleus. The decay mechanism of the compound nucleus will depends only upon the energy of excitation of the compound nucleus not on the mode of formation. Consequently, the angular distributions of the compound nuclear reaction are either completely or partially isotropic [26].

An interesting experimental verification was accomplished by S. N. Ghoshal in 1950 [19] as an example of the compound nucleus ^{64}Zn*, which can be formed through several reactions and decay in a variety of ways, as shown below. In the experiment two projectiles as α particle and proton were selected to make compound nucleus of ^{64}Zn*. For alpha-particle the target was $^{60}_{28}$Ni and for proton the target was $^{63}_{29}$Cu is selected.

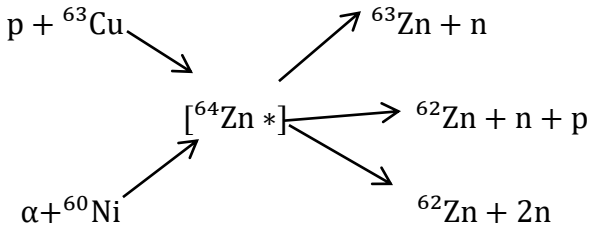

If the idea of the compound nucleus is valid and if one chooses the energy of the proton and of the incident α-particle to produce the same excitation energy, then the cross section for each one of the three exit channels should be independent of the way the compound nucleus is formed.

That is, the properties of the compound nucleus do not have any relationship with the nuclei that formed it. Due to the Bohr assumption, we can write the probability of formation of compound nucleus $\sigma_c(a)$, the probability of a decay of compound nucleus Y and emitted particle b of a nuclear reaction X(a, b)Y in the form [27];

$$\sigma(\alpha,\beta) = \sigma_c(\alpha)\mathrm{Gc}(\beta) \tag{2.7}$$

Where $\sigma_c(\alpha)$ is the cross section for the formation of compound system by the particle "α" incident up on the target nucleus X and $G_c(\beta)$ is the probability that the compound system C once formed, decays by emission of particle "β" leaving a residual nucleus Y. It is assumed that $G_c(b)$ is a pure number independent of the mode of formation of the compound nucleus. In a more reasonable way, if the sum is extended over all particles β which C can emit, it can be expressed as:

$$\sum_b G_c(\beta) = 1 \tag{2.8}$$

It is more important to specify the reaction X(a, b)Y in greater detail in terms of the cross section σ(α, β) corresponding to a specific entrance channel (α) and exit channels (β) as follows:

$$\sigma(\alpha,\beta) = \sigma_c(\alpha)\mathrm{G_c}(\beta) \tag{2.9}$$

According to the Bohr assumption, the disintegration of the compound system in to the different channels β, Y, etc. depends only on the energy E_c, the angular momentum J_c, and the parity of the compound system. In order to simplify our present consideration, the dependence properties of the compound system on the angular momentum J_c and the parity will be ignored in this section [14, 27]. Now introduce a few magnitudes which describe the disintegration of the compound system C. We begin with the mean life time τ (E_c) of C before disintegration and define the magnitude.

$$\Gamma(\mathrm{E_c}) = \frac{\hbar}{\tau E_c} \tag{2.10}$$

Which is ħ times the rate of disintegration per unit time, Γ is energy and, later on, will play the role of a level width.

We can therefore call it the total width of the state of C with excitation energy E_c. C can decay in to various channels and its total decay rate Γ can be subdivided in to decay rates referring to specific channels [14, 27].

$$\Gamma\,(E_c) = \sum_{\beta} \Gamma_{\beta}(\mathrm{E_c}) \qquad (2.11)$$

Where the sum is extended over all channels in to which C can decay, i.e., over all open channels. The specific decay rate Γ (E_c) is also a function of E_c and is called the partial width for the decay in to channel β. The magnitude Γ_β can also be defined as follow: If an assembly of N equal samples of the compound system C is arranged in such a way that, on the average, N system constant in time (i.e. as many compound systems decay are produced), then the number of decays in to channel β per unit time is given by;

$$\frac{N\Gamma_{\beta}}{\hbar} \qquad (2.12)$$

We can now express the branching probability in terms of the decay rates by the reaction.

$$\mathrm{G_c}(\beta) = \frac{\Gamma_{\beta}}{\Gamma} \qquad (2.13)$$

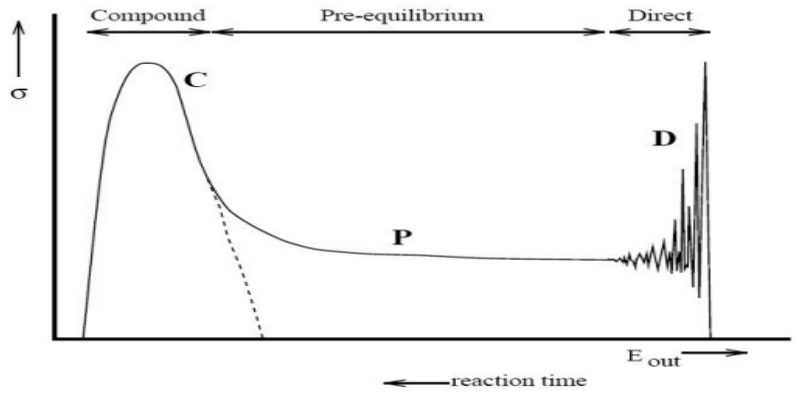

Figure.1.2.Schematic drawing of nuclear reaction [28].

Compound-nucleus model is description of atomic nuclei to explain nuclear reactions as a two-stage process comprising the formation of a relatively long-lived intermediate nucleus and its subsequent decay. It is very successful in explaining nuclear reactions induced by relatively low-energy bombarding particles (that is, projectiles with energies below about 50 MeV).

Compound-nucleus model includes fermi-gas model, generalized super fluid model, optical model and enhanced generalized super fluid model.

2.2.3.1. Fermi-Gas Model

The Fermi-gas model is a simple model used to describe the properties of a system of non-interacting fermions at thermal equilibrium. It is often used as a starting point for more sophisticated models that take into account the interactions between particles. It is also used to describe the behavior of nuclear matter, where the nucleons (protons and neutrons) can be modeled as non-interacting fermions. In the most recent versions of computer codes used for nuclear reaction calculations, the Fermi-Gas description is extensively used [29]. The density of intrinsic levels with spins J, parity π and excitation energy E_X is factorized in terms of state density and spin and parity dependence as [30].

$$\rho E_x, (J, \pi) = \rho(E_x)\, \rho(J, \pi) \qquad (2.14)$$

The energy dependence reads

$$\rho(E_x) = \frac{\exp S}{\sqrt{Det}} \qquad (2.15)$$

Where S is the entropy and Det is determinant of a matrix.

The spin and parity dependence is given by

$$\rho(J, \pi) = \frac{1}{2}\frac{2J+1}{\sqrt{8\pi\sigma^3}} \exp\left[\frac{(J+\frac{1}{2})^2}{2\sigma^2}\right] \qquad (2.16)$$

Where σ^2 the spin cut-off parameter and equal parity distribution is assumed. For the Fermi-Gas model the state equations determining the dependence of the excitation energy, entropy and other thermodynamic functions of a nucleus on its temperature T are.

$$E = aT^2; S = 2aT\,;\ \sigma^2 = \Im T\,; Det = 144a^3\frac{T^5}{\pi} \qquad (2.17)$$

Where a is the level density parameter and $\Im$ is the nuclear moment of inertia. To account for the odd-even ejects in nuclei, the excitation energy is replaced in calculations with the ejective energy.

$$U = E_X - \Delta \qquad (2.18)$$

Where, Δ is equal or closely related to the pairing energy. The well-known expression for the state density is

$$\rho^{FG}(E_X) = \frac{\sqrt{\pi}}{12a^{\frac{1}{4}}U^{\frac{5}{4}}} \exp(2\sqrt{aU}) \qquad (2.19)$$

$$\rho^{FG}(E_x, J, \pi) = \frac{2J+1}{48\sqrt{2}U^{\frac{5}{4}}\sigma^{\frac{3}{2}}a^{\frac{1}{4}}} \exp\left[2\sqrt{aU} - \frac{(J+\frac{1}{2})^2}{2\sigma^2}\right] \qquad (2.20)$$

These equations show that nuclear level densities in Fermi-Gas model depend on three parameters: a, σ and Δ.

2.2.3.2. Generalized Super Fluid Model

The Generalized Super Fluid Model (GSFM) is a theoretical framework that extends the compound nucleus model by incorporating the concept of superfluidity. In this model, the superfluid is treated as a single quantum mechanical entity, with all particles in the system behaving coherently and collectively. This model allows for the description of phenomena such as super fluidity, quantized vortices, and other unique properties exhibited by super fluids. The generalized superfluid model has been successful in explaining many experimental observations and is widely used in the study of superfluid systems. Generalized Super fluid Model is a default model used in EMPIRE-3.2 code to adjusted discrete levels and level density retrieved from reference input parameter library. This model use constant temperature model below critical energy and Fermi gas model above critical energy depend on the compound nucleus excitation energy. The phenomenological model is characterized by a phase transition of superfluid behaviour at low energy where the level density is strongly influenced by pairing energy term. The generalized super fluid model distinguishes between a low and high energy region [31]. The level density for the generalized super fluid model has been calculated as follows [32].

$$\rho(U) = \rho_{qp}U^1 K_{vib}(U^1) K_{rot}(U^1) \qquad (2.24)$$

Where the term ρqpU^1 denotes the density for quasi particle nuclear excitation and the terms $K_{vib}(U^1)$ and $K_{rot}(U^1)$represent rotational and vibrational enhancement factors at the U^1 effective energy of excitation.

The Generalized Super Fluid Model (GSFM) combines elements from both the Fermi Gas Model and the Superfluid Model, providing a more comprehensive description over a wide range of excitation energies as described below;

$$\rho(U) = \frac{\pi}{12}\frac{\exp(2\sqrt{a(U-\Delta)}}{a^{\frac{1}{4}}(U-\Delta)^{\frac{5}{4}}}\left(1+\sqrt{\frac{2}{\pi a(U-\Delta)}}\right) \qquad (2.21)$$

Where: $\rho(U)$ is the level density at excitation energy U, a is the level density parameter, U is excitation energy and Δ is the back-shift parameter is the excitation energy. This equation merges the high-energy behavior of the FGM with low-energy superfluid effects.

In Generalized Super Fluid Model (GSFM), the level density parameter a can be temperature-dependent:

$$a(T) = \tilde{a}\left[1+\frac{1}{T}\left(\frac{g_1}{1+\exp\left(\frac{T-T_1}{\Delta T_1}\right)}+\frac{g_2}{1+\exp\left(\frac{T-T_2}{\Delta T_2}\right)}\right)\right] \qquad (2.22)$$

Where $\tilde{a}$ is the asymptotic level density parameter, T is the nuclear temperature, and g_1, g_2, T_1, T_2, ΔT_1, ΔT_2 are fitting parameters.

The relationship between excitation energy U and temperature T in the GSFM is given by:

$$U = aT^2 \qquad (2.23)$$

This provides a basis for converting between energy and temperature in nuclear systems.

2.2.3.3. Enhanced Generalized Super Fluid Model

Enhanced Generalized Super Fluid Model (EGSFM) can be used to describe the behaviour of nucleons and other particles within the nucleus during the reaction process. This model takes into account the superfluid nature of the nucleus, where nucleons can move collectively in a coordinated manner, similar to a superfluid. The Enhanced Generalized Super Fluid Model considers various factors such as non-local interactions, quantum effects, and finite-range interactions between nucleons within the nucleus. These factors influence the dynamics of the compound nuclear reaction, affecting the formation of excited states, decay processes, and energy transfer within the system.

Enhanced Generalized Super fluid Model is a default model used in EMPIRE3.2 code to adjusted discrete levels and level density retrieved from reference input parameter library (RIPL- 3). The RIPL-3 includes the nuclear masses, discrete levels and decay schemes, neutron resonances, optical model parameters, level densities, gamma-ray strength function and fission barriers [31]. The model uses the super-fluid model below critical excitation energy and the Fermi gas model at energy above it. In non-adiabatic approximation, collective enhancements due to nuclear vibration and rotation are taking into account [33]. Hence it considers the shape of the nucleus in the dynamical situation. This deformation enters level densities formulas through moments of inertia and through the level density parameter that increases with increase in the surface of the nucleus. The level density parameter in EGSFM is a function of excitation energy U and can also be temperature-dependent:

$$a(U) = \tilde{a}\big(1 + f(U)\big) \qquad (2.25)$$

where $\tilde{a}$ is the asymptotic level density parameter, a(U) is a function incorporating shell and pairing corrections. The level density ρ (U) in EGSFM can be expressed as;

$$\rho(U) = \frac{\exp(2\sqrt{a(U - \Delta U)}}{12\sqrt{2}a^{\frac{1}{4}}(U - \Delta U)^{5/4}} \qquad (2.26)$$

Where ΔU accounts for pairing and shell effects.

2.2.3.4. Optical Model (OM)

The compound formation process relies on the optical model, nuclear level density, and gamma-ray strength function. Traditionally, the optical model is developed by assuming specific functional forms and adjusting their parameters to achieve a close match with experimental data. This method, known as the phenomenological approach, remains widely used because it can provide a highly accurate description of experimental data, often achieving total cross-section accuracy within less than 1%. However, this approach is heavily dependent on the availability of experimental data. A key advantage of a well-constructed optical model is its ability to reliably predict quantities for energies and nuclides without existing measurements. It also significantly influences the evaluation of various channels, such as transmission coefficients for compound nuclei and the pre-equilibrium model.

This includes the distorted wave functions used for direct inelastic reactions and transitions to the continuum, which describe statistical multi-step direct reactions. In this model, we represent the scattering in terms of a complex potential V(r**)**:

$$V(r) = U(r) + i\,W(r) \qquad (2.27)$$

Where the real functions U(r) and iW(r) are selected to give the potential its proper radial dependence. The real part, U(r), is responsible for the elastic scattering; it describes the ordinary nuclear interaction between target and projectile and may therefore be very similar to a shell-model potential. The imaginary part iW(r) is responsible for the absorption [17].The phenomenological optical model potential for incident neutrons and protons is defined as [33]:

$$V(r) = V_c(r) + Uf_s(r) + iW_s(r) + \left(\frac{\hbar^2}{m_x c}\right)^2 \frac{1}{r} U_s \frac{df_s}{dr} l.s \qquad (2.28)$$

Where $V_c(r)$ is the electrostatic potential of the nucleus included only in the proton optical Potential. The terms U, W, and U_s denote the real potential depth, the imaginary potential depth, and the spin-orbit potential depth, respectively. The quantity l.s represents the scalar product of the intrinsic and orbital angular momentum operation and is given as: $l.s = l$ for $j = l + \frac{1}{2}$ and $l.s = -(l+1)$ for $j = l - \frac{1}{2}$. Due to the short range interaction of nucleon-nucleon, the potential $Uf_s(r)$which is approximately the sum of nucleon-nucleon interactions has the same behaviors. Nucleons in the core of the nucleus primarily interact with their nearest neighbors. Because of this saturation of nuclear forces, the potential $Uf_s(r)$ is uniform within the nucleus and decreases exponentially in the surface region. The variations of the real part of the interaction potential are approximated by a Wood-Saxon function:

$$f_s(r) = \frac{1}{1+\exp\left[\frac{r-R_i}{a_i}\right]} \qquad (2.29)$$

Where the geometry parameters are the radius $R_i = r_i A^{\frac{1}{3}}$ with A the atomic mass number, the diffuseness a_i for each component. The form factor g_r is derived function of Woods-Saxon situated at the surface of the nucleus:

$$g_r = 4a\frac{df(r)}{dr} \qquad (2.30)$$

When complex nuclear potential is introduced in the radial part of Schrödinger equation, the total elastic scattering is defined as;

$$\Sigma_T = \sigma_R + \sigma_E \qquad (2.31)$$

2.4. Nuclear reaction cross section

Reaction cross-section is a term used in nuclear physics to describe the probability that an atomic nucleus will exhibit one of the following reactions: absorption, scattering, or fission, in response to a specific incident particle. Because interactions in a nuclear reaction take place with individual target nuclei independently of each other, it is useful to refer to the probability of a nuclear reaction for one target nucleus. It is a measure of the quantity of probability for a particular reaction to occur. This quantity should be easily measurable and also theoretically calculable, so that we can compare the experimental results with the theoretical calculations. It is helpful to refer the probability of a nuclear reaction to a single target nucleus because interactions in a nuclear reaction occur with individual target nuclei independently of one another [22]. To define the probability of a reaction, consider an experiment where a thin slab of target material is struck by a monoenergetic beam consisting of particles uniformly distributed over an area per unit time.

When a nuclear reaction occurs, producing particles per unit time, we can imagine that each target nucleus has an associated area perpendicular to the incident beam. If the center of a bombarding particle strikes within this area, a hit and subsequent reaction occur. Conversely, if the center of the bombarding particle misses this area, no reaction takes place. So the quantity σ is defined as cross-section, and it gives a measure of the reaction probability per target nucleus. It is a fictitious area that need not be related to the cross-sectional area (πr^2) of the struck nucleus. It is also possible to describe the reaction probability by the ratio, however, this quantity depends on the target density as well as its thickness Δx, whereas σ is associated with an individual target nucleus. The probability that any one bombarding particle has a hit is equal to and is also equal to the projected total cross-section of all target nuclei lying within the area A, as seen along the beam direction, divided by A. If there are target nuclei per unit volume in the target material, such nuclei are within reach of any bombarding particle in the beam. Each target nucleus has an associated cross-section so;

$$\frac{N}{I} = \frac{nA\Delta x\sigma}{A} \tag{2.32}$$

Using this relation we can define cross-section by writing;

$$\sigma = \frac{N}{\frac{I}{A}nA\Delta x} \tag{2.33}$$

Units of reaction cross-sections are the units of area. These cross-sections are normally very small ~10^{-27} to 10^{-28} m^2. Since this value is small so it is convenient to use a unit called barn. 1barn (b) = 10^{-28} m^2. Smaller units of cross sections are millibarn and microbarn.

2.4.1. Partial wave analysis of reaction cross-section

Under general assumptions, the nuclear reaction cross-section can be explained by wave mechanical theory [32]. Let us examine a neutron beam that is collimated and traveling in the direction of z. This neutron beam can be considered as a plane wave exp(ikz) [32].

$$\psi_{inc} = e^{ikz} \tag{2.34}$$

The plane wave can be explained in terms of Bessel's function and spherical harmonic of various value ℓ.

$$e^{ikz} = \sum_{\ell=0}^{\infty} i^{\ell}\,(2\ell+1)j_{\ell}(kr)p_{\ell}(\cos\theta) \tag{2.35}$$

$$j_{\ell}(kr) = \frac{\sin(Kr - \frac{\ell\pi}{2})}{kr} \tag{2.36}$$

$$p_{l(\cos\theta)} = \Upsilon_{l,0(\theta)}\sqrt{\frac{4\pi}{2l+1}} \tag{2.37}$$

For r→ ∞ then the Bessel function $j_{\ell}(kr) = \frac{\sin(kr-\frac{\ell\pi}{2})}{kr}$

$$\psi_{inc} = \frac{1}{kr}\sum_{l=0}^{\infty} i^{\ell}\,(2\ell+1)\sin(kr - \frac{\ell\pi}{2}p_{\ell}(\cos\theta) \tag{2.38}$$

$$\psi_{inc} = \frac{1}{2ikr}\sum_{l=0}^{\infty}(2l+1)\left\{e^{-i\left(kr-\frac{l\pi}{2}\right)} - e^{i\left(kr-\frac{l\pi}{2}\right)}\right\}p_{\ell}(\cos\theta) \qquad (2.39)$$

The first terms which is represented by $e^{-i(kr-\frac{\ell\pi}{2})}$ is the incoming (incident) spherical wave and the second terms represents by $e^{i(kr-\frac{\ell\pi}{2})}$ is the outgoing (reflected) spherical wave.

If the reflected (outgoing wave) are affected by in amplitude as well as in phase, we have an inelastic scattering process which can be represented by the wave equation:

$$\psi_r = \frac{1}{2ikr}\sum_{l=0}^{\infty}(2l+1)i^{\ell}\,p_{\ell}(\cos\theta)\left(\eta_{\ell}e^{i\left(kr-\frac{\ell\pi}{2}\right)}\right) \qquad (2.40)$$

Where η_{ℓ} is a complex constant which contain the effect of the scattering center. Its real part gives the change in amplitude and its imaginary part gives the change in phase. It can be represented by:

$$\eta_{\ell} = |\eta_{\ell}|e^{i\delta_{\ell}} \qquad (2.41)$$

Where $e^{i\delta_{\ell}}$ the phase is shift, and η_{ℓ} is the amplitude

Now the phase is changing (phase shift) then scattering is taking place. The scattering wave can be written as

$$\psi_{sc} = \psi(r) - e^{ikz} \qquad (2.42)$$

$$\psi_{sc} = \sum_{\ell=0}^{\infty}\frac{1}{2kr}(2\ell+1)i^{\ell+1}1 - \eta_{\ell}\left(e^{i\left(kr-\frac{\ell\pi}{2}\right)}\right)p_{\ell}(\cos\theta) \qquad (2.43)$$

The scattered wave can be also written in terms of scattering amplitude as follows.

$$\psi_{sc} = \frac{f(\theta)}{r}e^{ikr} \qquad (2.44)$$

f(θ) is the scattering amplitude ,than to get the value of f(θ) simply compare the above two equation

$$f(\theta)\frac{e^{kr}}{r} = \sum_{\ell=0}^{\infty}\frac{1}{2kr}(2\ell+1)i^{\ell+1}1-\eta_{\ell}\left(e^{i\left(kr-\frac{\ell\pi}{2}\right)}\right)p_{\ell}(\cos\theta) \qquad (2.45)$$

$$f(\theta) = \sum_{\ell=0}^{\infty}\frac{i^{\ell+1}}{2kr}(2\ell+1)e^{\frac{-i\ell\pi}{2}}(1-\eta_{\ell})p_{\ell}(\cos\theta) \qquad (2.46)$$

For any value of ℓ, $i^{\ell}\ e^{\frac{-i\ell\pi}{2}} = 1$, then the above equation becomes,

$$f(\theta) = \frac{1}{2kr}\sum_{\ell=0}^{\infty}(1-\eta_{\ell})p_{\ell}(\cos\theta)(2\ell+1) \qquad (2.47)$$

For elastic scattering there is no loss of incident particles $|\eta_{\ell}|^2 = 1$ this means there is no change in amplitude between the incident and scattering wave. The scattering amplitude is given by;

$$f(\theta) = \frac{1}{2ikr}\sum_{\ell=0}^{\infty}(2l+1)(e^{2i\delta_l}-1)p_l\cos\theta \qquad (2.48)$$

For inelastic reaction $|\eta_{\ell}|^2 < 1$ there is change in amplitude.

The number of scattering particles (N_{sc}) through a solid angle dΩ is given by;

$$N_{sc} = \frac{\hbar}{2im}\int_{-\infty}^{\infty}\int_{-\infty}^{\infty}\left(\frac{\partial\psi_{sc}}{\partial r}\psi_{sc}^{*} - \frac{\partial\psi^{*}_{sc}}{\partial r}\psi_{sc}\right)r^2\,d\Omega$$

$$N_{sc} = v\,|f(\theta)|^2 d\Omega \qquad (2.49)$$

Where 'm' is the mass of the scattering particles and r^2 is the radius of the sphere with solid angle dΩ. The scattering cross section is given by

$$\sigma_{sc} = \frac{N_{sc}}{flux} \qquad (2.50)$$

$$\sigma_{sc} = \frac{v\iint|f(\theta)|^2}{v}d\Omega \qquad (2.51)$$

$$\sigma_{sc} = \iint|f(\theta)|^2\,d\Omega \qquad (2.52)$$

$$\sigma_{sc} = \frac{\pi}{k^2}\sum_{l=0}^{\infty}(2l+1)\mid 1-\eta_{\ell}\mid^2 \qquad (2.53)$$

But $p=\frac{\hbar}{\lambda}=\hbar k$

$$\sigma_s = \pi\lambda^2(2l+1)|1-\eta_{\ell}|^2 \qquad (2.54)$$

Similarly reaction cross section is equal to negative of probability current. The negative sign indicates the direction of the wave.

$$\sigma_r = \frac{N_r}{v} = \frac{\pi}{k^2}\sum_{l=0}^{\infty}(2l+1)(1-\mid \eta_{\ell}\mid^2) \qquad (2.55)$$

$$\sigma_r = \pi\lambda^2(2l+1)(1-|\eta_{\ell}|^2) \qquad (2.56)$$

If η_{ℓ} = 0, there is no change in amplitude of the wave, so there is no reaction (σ_r) but scattering may be. On the other hand if η_{ℓ} =1, both reaction and scattering are not happens. If η_{ℓ} = -1 there is no reaction but there is the possibility of maximum scattering. If η_{ℓ}=0, we have maximum reaction (absorption) and scattering also occur. The total reaction cross section is equal to the sum of the scattering cross section and reaction cross section.

$\sigma_t = \sigma_{sc}+\sigma_r$ From the above two equation;

$$= \pi\lambda^2(2\ell+1)[(1-|\eta_{\ell}|^2)+|1-\eta_{\ell}|^2 \qquad (2.57)$$

$$= \pi\lambda^2(2\ell+1)[(1-\eta_{\ell}\eta_{\ell}^{*}+(1-\eta_{\ell})(1-\eta_{\ell}^{*})] \qquad (2.58)$$

$$=\pi\lambda^2(2\ell+1)[2-\eta_{\ell}-\eta_{\ell}^{*}] \qquad (2.59)$$

$$=\pi\lambda^2(2\ell+1)[2-(Re\eta_{\ell}+Img\eta_{\ell})] \qquad (2.60)$$

$$\sigma_t = \pi\lambda^2(2\ell+1)[2-2Re\eta_{\ell}] \qquad (2.61)$$

But $\eta_{\ell} = |\eta_{\ell}|e^{2i\delta_{\ell}}$

For the real part $\eta_{\ell} = Re\eta_{\ell} = \cos 2\delta_{\ell}$, hence 1- $Re\eta_{\ell} = 2\sin^2\delta_{\ell}$

Thus,

$$\sigma_t = 4\pi\lambda^2(2l+1)\sin^2\delta_l \tag{2.62}$$

When $|\eta_\ell|=0$

$$\sigma_{sc} = \sum_{\ell=0}^{max} \pi\lambda^2(2\ell+1) \tag{2.63}$$

$$\sigma_{rmax} = \sum_{\ell=0}^{max} \pi\lambda^2(2\ell+1) \tag{2.64}$$

Then total reaction cross section is

$$\sigma_t = \sigma_{sc} + \sigma_{rmax} \tag{2.65}$$

$$= \sum_{\ell=0}^{max} \pi\lambda^2(2\ell+1) + \sum_{\ell=0}^{max} \pi\lambda^2(2\ell+1) \tag{2.66}$$

$$= 2\pi\lambda^2 \sum_{\ell=0}^{max} (2\ell+1) \tag{2.67}$$

$$= 2\pi\lambda^2(\ell_m+1)^2) \tag{2.68}$$

Where, $l_m = \frac{R}{\lambda}$

$$= 2\pi\lambda^2(\frac{R}{\lambda}+1)^2 \tag{2.69}$$

$$= 2\pi\lambda^2 \frac{(R+\lambda)^2}{\lambda^2} \tag{2.70}$$

$$= 2\pi(R+\lambda)^2 \tag{2.71}$$

For high energy $R \gg\gg \lambda$

$$\sigma_T = 2\pi R^2 \tag{2.72}$$

This implies that total cross-section is twice of the geometrical cross-section of the nucleus.

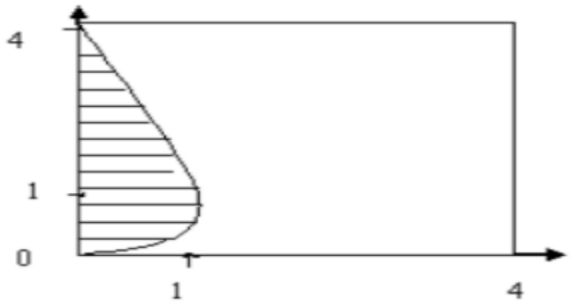

Figure.2.3. Possible values of scattering and reaction cross-section.

The shaded region is possible values of the cross section, taken from ref [26].

2.5. Thick target yield

Thick target yield is a specific type of production yield that applies to reactions where a thick target is used. It is a macroscopic quantity reflected by nuclear reactions and matter properties of targets. A thick target refers to a target material with a thickness sufficient enough to stop most or all incident particles. Large-scale, high-current medical systems that can generate enhanced yields of radioisotopes require the development of experimental thick target yields and excitation functions, or energy-dependent isotope production cross sections [34]. The thick target yields obtained in routine production (practical yields) are usually lower than those measured under well-defined conditions (nominal yields) due to various possible reasons such as loss of the beam particles, variation of the beam intensity, loss of the reaction product (e.g., evaporation, sublimation, recoil effect), or density reduction and radiation damage effects of the target material [35]. However, the nominal yield measurements are helpful in verifying the excitation functions [36]. Under the supervision of the International Atomic Energy Agency (IAEA), the International Network of Nuclear Reaction Data Centers (NRDC) has collected experimental excitation functions and thick target yields for charged-particle induced radioisotope production from over 800 experimental works, which are now stored in the Experimental Nuclear Reaction Data Library (EXFOR) [37].

In order to retrieve and analyses experimental thick target yields of a specific type from EXFOR efficiently and appropriately, each experimental data set must be properly tagged not only by the reaction (i. e, target, beam particle, product) but also by the definition of the thick target yield.

The yield calculation for medically important radionuclides is crucial component of nuclear medicine and radiopharmaceutical production. Thick target yield are influenced by various factors such as beam energy, beam current, reaction cross-section, and half-life of radionuclides. These factors determine which nuclear reaction pathway will be most efficient for producing a specific radionuclide. For example, one commonly used nuclear reaction in medical radioisotope production is (p, n) or proton-induced nuclear reactions. The thick target yields for these reactions can vary significantly depending on factors like proton energy and cross-section data for specific isotopes. To optimize production yields and maximize efficiency in medical radioisotope production, extensive research and development efforts are undertaken to identify optimal conditions for each specific radionuclide. This includes studying different irradiation parameters, selecting appropriate targets, and optimizing beam characteristics.

The term thick target yield is used to characterize the produced radioisotopes quantitatively. The thick target yield for the production of medically important radionuclide via the investigated reaction channel has been calculated by using a known Equation [38],

$$Y = \frac{N_A H \lambda_p}{M_T Z_{proj} e} \int_{E_2}^{E_1} \left(\frac{dE}{d(\rho x)}\right)^{-1} \sigma(E) dE \qquad (2.73)$$

Where N_A= Avogadro number, H = Isotopic abundance of target, M_T = mass number of target element, Z_{proj} = atomic number of projectile, e = electric charge, E_1 and E_2 are the incident and outgoing energies of the projectile, $\frac{dE}{d(\rho x)}$ = stopping potential, $\sigma(E)$ = cross section and λ_p= decay constant.

If the product is radioactive with decay constant λ and the number of the produced nuclei following deposition of unit induced electric charge *y*, then the number of the produced nuclei present in the sample $N(t)$ satisfies;

$$\frac{dN(t)}{dt} = \frac{dY}{dt} - \lambda N(t) = I_0 y - \lambda N(t) \qquad (2.74)$$

And its solution is

$$N(t) = I_0 y \left(\frac{1 - e^{-i\lambda t}}{\lambda}\right) \qquad (2.75)$$

The activity of the sample material per unit current at t is therefore

$$\frac{\lambda N(t)}{I_0} = y\left(1 - e^{-i\lambda t}\right) = a(t) \qquad (2.76)$$

which is defined as the End -Of-Bombardment (EOB) thick target yield.

For a very long irradiation $\lambda t \gg 1$ (e. g., irradiation is much longer than the half-life of the product), the production rate and decay rate of the product are in equilibrium, and the EOB thick target yield becomes;

$$a(t \to \infty) = y = a_{sat} \qquad (2.77)$$

which is defined as the saturation thick target yield.

Equation (2.77) shows that the thick target product yield y and the saturation thick target yield a_{sat} are essentially the same except for their interpretation: y is the number of the produced nuclei per unit induced electric charge (e. g., $1\text{nuclei}/\mu\text{C}$), while $a(t)$ and a_{sat} are the decay rates of the product per unit current (e. g., $\text{MBq}/\mu\text{A}$). Note that $1\text{nuclei}/\mu\text{C} = 1\text{MBq}/\mu\text{A}$. The thick target yield is expressed as activity per electric charge, in the unit of Bq/C. The electric charge is convertible to the product of current and time and its unit is Bq/As. The thick target yield in the unit of $\text{MBq}/\mu\text{Ah}$ is widely used.

CHAPTER THREE

COMPUTER CODE AND FORMULATIONS

Theoretical production cross sections and yield calculations based on nuclear reaction models significantly develop reliable radionuclides production data [39] and predict reaction cross-sections without experimental data. In this work, the production cross section and yield of medically important radionuclides, such as ^{68}Ga and ^{64}Cu, generated during irradiation of ^{66}Zn with alpha energy between ≈ 10 - 40 MeV were studied using the computer codes COMPLETE, TALYS1.95(G), and EMPIRE 3.2.

3.1 COMPLETE code

Production cross-sections and yield calculations have been predicted using COMPLET code, an enhanced and advanced version of the ALICE code family with extra physics, corrections, and features. The Weiss Kopf-Ewing model for the statistical component and the geometry-dependent hybrid Blann model for pre-equilibrium (PE) emission are both included in ALICE-IPPE [3]. This code has successfully predicted numerous nuclear data, particularly for producing medical radionuclides (Amanuel, 2021). In the ALICE/ASH code, level densities of residual nuclei play an important role in deciding the shapes and absolute value of excitation functions. The Fermi density distribution can be used to calculate the level densities of the nuclides.

$$\rho(E) = \frac{\pi^{\frac{1}{2}} e^{2\sqrt{aE}}}{12\alpha^{\frac{1}{4}} E^{\frac{5}{4}}} \qquad (3.1)$$

Where; "E" is the excitation energy and "a" the level density parameter. The level density parameter obtained by the experiment shows a linear dependence on the mass number of the compound nucleus. In general, it is expressed.

$$a = \frac{A_{CN}}{K} \qquad (3.2)$$

Where A_{CN} is the mass of the compound nucleus, and K is the free constant. The values of K vary to find the best-fitted value of K. A sensitive input parameter in the COMPLET code is the exciton number (n_o), which describes the particles in the initial configuration.

Exciton number (n_o) is described by the number of neutrons (n), the number of protons (p) in excited states, and the number of holes (h) after the first projectile-target interaction. It is equal to the sum of n, p and h. The exciton number (n_o) also varies to find the best-fitted value.

3. 2. TALYS1.95 (G)

TALYS1.95 (G) code is an advanced version of the TALYS-1.95 code family [30]. It was written in FORTRAN computer language. Additionally, we insist on full FORTRAN77 compatibility for this version since it is the last one. Nuclear reactions involving neutrons, photons, protons, deuterons, tritons, 3He, and α-particles in the 1 keV–200 MeV energy range as well as target nuclides of mass 12 and heavier are analyzed and predicted using the TALYS1.95 (G) code. The TALYS1.95 (G) code includes the optical model, direct model, CN model, PE emission, and fission models. The Hauser–Feshbach formalism is used to describe the emission of equilibrium particles [40]. TALYS1.95 (G) is essentially useful for two purposes. The first one is nuclear physics, which is employed in examining experiments involving nuclear reactions. We are able to constrain our models by gaining insight into the fundamental interactions between particles and nuclei through the comparison of theory and experiment. Second, as a nuclear data tool, TALYS1.95 (G) can produce nuclear data on energy and angle range that is user-defined for all open reaction channels.

Local energy-dependent parameters can vary TALYS 1.95 cross-sections to fit the experimental data using optical model parameters and level density parameters. In addition to the semi-microscopic nucleon-nucleus spherical optical model potential [41], TALYS calculations were performed using the phenomenological Optical Model Parameter (OMP). Pre-equilibrium models describe the continuum spectra's high-energy parts (E >25 MeV). In essence, these models are single-particle systems. TALYS calculations incorporate both classical and quantum mechanical models of pre-equilibrium reactions. TALYS1.95's input parameters (masses, optical model parameter, level densities) are also taken from the Standard RIPL-3 library (EXFOR). The input parameters for TALYS are changed to achieve the best fit for the experimental data while staying within the specified bounds.

3.3. EMPIRE3.2

The computer code EMPIRE 3.2 [42] is modular in nature, includes multiple nuclear models, and is designed for calculations of cross-sections for major reaction mechanisms, including direct, pre-equilibrium, and compound nucleus ones. In this code, a projectile can be a neutron, proton, any ion (including heavy ions), or a photon. The energy range for heavy-ion-induced reactions reaches several hundred MeV, while for neutron-induced reactions, it starts at the beginning of the unresolved resonance region (≈ keV). The statistical Hauser-Feshbach model [40] with γ-cascade and width-fluctuations describes the decay of compound nuclei, while the Exciton model describes the pre-equilibrium emission. In the current EMPIRE code calculations, the Enhanced Generalized Superfluid Model (EGSM) is the default level density model. This model was selected because it has been very successful in the predictions of excitation function.

In Empire, a wide range of energies are available for calculation. This code can be used for theoretical investigations of nuclear reactions and evaluating nuclear data. The input parameters were taken from a comprehensive library of input parameters, "RIPL-3 library". It covers nuclear masses, optical model parameters, ground state deformations, discrete levels, decay schemes, and level densities. EMPIRE is intended to be a general, flexible, and easy-to-use tool for basic research and evaluation of nuclear data. It also a possibility of combining several theoretical approaches choosing among alternative input parameter and evaluating extended set of observation.

3.4. Weiss Kopf-Ewing Formulation

The compound nucleus states are excited separately at low incident energies, and each generates a resonance in the cross-section that can be explained by the Breit-Winger theory [43]. As the incident energy increases, compound nucleus states of higher energy are excited, which are closer to gathering and of increasing width. They eventually overlap, making it impossible to identify the individual Weiss-Kopf-Ewing theory of compound nucleus reactions that precede the Hauser-Feshbach theory [43]. The energy average of the cross-section does not exhibit these fluctuating features because the amplitudes are complex functions with random modulus and phase. The theory predicts that the energy average of the cross-sections will exhibit weak energy dependence.

A reaction that moves from the first channel, α, via the compound nucleus to the last channel, β, is needed to accomplish this. The cross-section is then given by the independence of the CN's formation and decay, assuming that the compound nucleus is formed at a different angular momentum J [19].

$$\sigma_{\alpha\beta} \approx \sigma_{CN}(\alpha)\frac{\Gamma_\beta}{\Gamma} \tag{3.3}$$

Where $\sigma_{CN}(\alpha)$ is the cross-section for the formation of the CN and, Γ_β and Γ are respectively, the energy average width for the decay of the CN in channel β and the energy averaged total width. From reciprocity theorem we can have

$$g_\alpha k_\alpha^2 \sigma_{\alpha\beta} = g_\beta k_\beta^2 \sigma_{a\beta} \tag{3.4}$$

Where $g_\alpha = 2i_\alpha + 1$ and $g_\beta = 2i_\beta + 1$ are the statistical weights of the initial and final channels, i_α and i_β are the spin of the projectile and the ejectile, and k_α and k_β are their wave numbers. This gives,

$$k_\alpha^2 \sigma_{CN}(\alpha)\Gamma_\alpha = g_\beta k_\beta^2 \sigma_{CN}(\alpha)\Gamma_\beta \tag{3.5}$$

or equivalently

$$\frac{\Gamma_\alpha}{g_\alpha k_\alpha^2 \sigma_{CN}(\alpha)} = \frac{\Gamma_\beta}{g_\beta k_\beta^2 \sigma_{CN}(\beta)} \tag{3.6}$$

Since the channels α and β are chosen arbitrarily, this relation holds for all possible channels so

$$\Gamma_\alpha \propto g_\alpha k_\alpha^2 \sigma_{CN}(\alpha) \tag{3.7}$$

Since the total width is obtained by summing the Γ_α of overall open channels

$$\Gamma = \Sigma_\alpha \Gamma_\alpha \tag{3.8}$$

The cross-section in (3.4) becomes

$$\sigma_{\alpha\beta} = \sigma_{CN}(\alpha)\frac{g_\beta k_\beta^2 \sigma_{CN}(\beta)}{\Sigma_\alpha g_\alpha k_\alpha^2 \sigma_{CN}(\alpha)} \tag{3.9}$$

Ejectiles with energy in the range ε_β to $+d\varepsilon_\beta$ leave residual nucleus with energies in the range $u_\beta + du_\beta$, were

$$u_\beta = E_{CN} - B_\beta - \varepsilon_\beta \qquad (3.10)$$

E_{CN} and B_β are respectively the CN energy and the binding of the ejectile in the CN. Introducing the density of levels of the residual nucleus ω (u_β) Eq (3.10) becomes

$$\sigma_{\alpha\beta} = \sigma_{CN}(\alpha)\frac{g_\beta k_\beta^2 \sigma_{CN}(\beta)\omega(u)du_\beta}{\Sigma_\alpha \int_0^{\Sigma_\alpha max} g_\alpha k_\alpha^2 \sigma_{CN}(\alpha)\omega(u_\alpha)du_\alpha} \qquad (3.11)$$

Or, since, $k^2=2m\varepsilon$

$$\sigma_{\alpha\beta}d_\beta = \frac{\sigma_{CN}(\alpha)\ (2i_\beta+1)u_{\beta_\beta}\ \sigma_{CN}(\beta)\omega(u_\beta)du_\beta}{\Sigma_\alpha \int_0^{\Sigma_\alpha max}(2i_\alpha+1)u_{\alpha_\alpha}\ \sigma_{CN}(\alpha)\omega(u_\alpha)du_\alpha} \qquad (3.12)$$

Where U_a is the reduced mass of the ejectile α, this is the Weisskopf-Ewing formula for the angle integrated cross-sections. The corresponding general expression for the particle emission width is,

$$\Gamma_\beta = \frac{1}{\rho_{CN\ E_{CN}}} . \frac{(2i_\beta+1)}{\pi^2\hbar^2}\ \rho_\beta(\beta)\omega(u_\beta)d\varepsilon_\beta \qquad (3.13)$$

After the compound nucleus forms at certain excitation energy and with a certain cross-section, the COMPLET code predicts the reaction cross-sections using the above-mentioned equations. The evaporation of a neutron, proton, alpha, and deuteron is then carried out using the Weisskopf calculation with a grid size of 1 MeV, storing the remaining nucleus population in the appropriate bin. After the compound nucleus emits neutrons, control shifts to the A-1 bin. This bin can also result in Proton, deuteron, and alpha particle emission. The residual nuclei obtained from the emission of particles above are stored in the respective bins. The code redistributes that cross-section similarly by using the millibarn value in the highest energy bin A-1. The process then continues until all of the cross-section has been redistributed and summed in the proper bins of the residual nuclides. After that, the control drops to the next residual excitation bin. Across the A, this logic is repeated as far as an input parameter requests. After this, the control comes down in Z to the nucleus A-1, Z-1 and repeats the process till all calculations are completed for each input parameter.

3.5. Hauser-Feshbach Formulation

The cross-section of reactions that go through a lot of different compound nucleus states is provided by the Hauser-Feshbach theory. In this section, we will examine the reactions leading to a single final state in the residual nucleus and expand the theory to include reactions leading to continuum states. An expression for the total cross-section of a compound nucleus reaction can be obtained by applying the Bohr independence hypothesis in conjunction with a few other simplified assumptions [44]. The formation of the compound nucleus in states with varying J and parity is considered in this theory. Let us consider the case of a reaction leading from the initial channel α to the final channel β [19].

$$\Sigma_{\sigma\beta} = \Sigma_{J,\pi}\sigma_{\alpha\beta}^{J\pi} \tag{3.14}$$

Averaging over the energy, one further assumes the Bohr independent hypothesis holds for each $\sigma_{\alpha\beta}^{J\pi}$ thus,

$$\sigma_{\alpha\beta}^{J\pi} = \sigma_{CN}^{J\pi}(\alpha)\frac{\Gamma_{\beta}^{J\pi}}{\Gamma^{J\pi}} \tag{3.15}$$

Repeating the procedure used to obtain the Weisskopf-Ewing expression gives

$$\Gamma_{\beta}^{J\pi} \propto g_{\alpha}^{2}\sigma_{CN}^{J\pi}(\alpha) \tag{3.16}$$

Where now $g_{\alpha} = (2i_{\alpha} + 1)(2I_{\alpha} + 1)$ and i_{α} and I_{α} are, respectively, the projectile and target spin in channel. If the process of pre-equilibrium emission is not taken in to consideration, the compound nucleus formation cross section (σ_{CN})

$$\sigma_{CN} = \Sigma_{J,\pi}\sigma_{CN}^{J\pi} \tag{3.17}$$

And the corresponding optical model reaction cross-section

$$\sigma_{R} = \frac{\pi}{K^{2}}\Sigma_{\ell}(2\ell + 1)T_{\ell} \tag{3.18}$$

Considering J independent transmission coefficients $T_{\ell} = 1 - |S\bar{\ell}|^{2}$, the reaction cross-section may also be written as,

$$\sigma_{R} = \frac{\pi}{k^{2}}\sum_{\ell=0}^{\infty}\Sigma_{s=|I-1|}^{I+1}\Sigma_{J=|\ell-s|min}^{\ell+1}\frac{(2J + 1)T_{\ell}}{(2i + 1)(2I + 1)} \tag{3.19}$$

Where s is the channel spin s=I+i. by rearranging the summation over different indexes one gets;

$$\sigma_{CN} = \sigma_R \frac{\pi}{k^2} \Sigma_J \frac{(2J+1)T_\ell}{(2i+1)(2I+1)} \sum_{s=|I-i|\ min}^{I+i} \sum_{l=|I-i|\ min}^{J+S} T_l \qquad (3.20)$$

By comparing Eq. (3.14) and Eq. (3.20) one can gets,

$$\frac{\Gamma_\alpha^{J\pi}}{\Gamma^{J\pi}} = \frac{\Gamma_\alpha^{J\pi}}{\Sigma_\alpha \Gamma_\alpha^{J\pi}} = \frac{\Sigma_{s,\ell} T_{\ell(\alpha)}}{\Sigma_\alpha \Sigma_{s,\ell} T_{\ell(\alpha)}} \qquad (3.21)$$

Now, the cross-sections in Eq. (3.15) for the transition from the initial channel α to the final channel β may be written as,

$$\sigma_{\alpha\beta} = \frac{\pi}{k^2} \Sigma_J \frac{(2J+1)}{(2i_\alpha+1)(2I_\alpha+1)} \frac{\Sigma_{s,\ell} T_{\ell(\alpha)} \Sigma_{s,\ell} T_{\ell(\beta)}}{\Sigma_\alpha \Sigma_{s,\ell} T_{\ell(\alpha)}} \qquad (3.22)$$

This is the simplest form of the Hauser-Feshbach formula for the energy-averaged, angle-integrated cross-section of statistical reactions (reaction cross-section leading to a single final state). If one interested on the cross section for populating all the available final states cross ponding to a given particles with energy between ε_β and $\varepsilon_\beta + d\varepsilon_\beta$, and a residual nucleus with energy between U_β and $U_\beta + dU_\beta$, where $U_\beta = E_{CN} - B_\beta - \varepsilon_\beta$, the formula is adapted accordingly.

Consider the spin dependent level density of residual nucleus with energy U_β and spin I_β might be factorized into the product of an energy dependent and a spin de-pendent term.

$$\omega_\beta(u_{\beta,I_\beta}) = U_\beta(\omega_\beta) F(I_\beta) \qquad (3.23)$$

$$F(I) = (2I+1) \exp\left(-\frac{I(I+1)}{2\sigma^2}\right) \qquad (3.24)$$

ω_β (u_β) Refers to level density, therefore the Eq (3.19) becomes;

$$\sigma_{\alpha\beta} = \frac{\pi}{k^2} \times \frac{\sum_{s,l} T_l(\alpha) \sum_{s,l} T_l(\beta) \sum_{I,\beta} \rho_\beta(U_\alpha)(2I_\beta+1) \exp(-\frac{I_\beta(I_\beta+1)}{2\delta^2\beta})}{\sum_\beta \int_0^{Emax\beta} \sum_{s,l} T_l(\beta) \sum_{I,\beta} \rho_\beta(U_\beta)(2I_\beta+) \exp(\frac{I_\beta(I_\beta+1)}{2\alpha^2\beta})} \qquad (3.25)$$

This expression is the width for the decay of CN in the state of energy E and spin J.

3.6. Pearson's correlation coefficient

Pearson's correlation coefficient is a statistical measure that quantifies the strength and direction of the linear relationship between two variables.

Pearson's correlation coefficient (R) was used to assess the correlation between the total cross-section results from the experiment and the theory. One of the most common analytical tools data analysts use is the computation of correlation coefficients between paired data variables. Pearson's correlation coefficient is a de facto standard in most fields; a correlation coefficient quantifies the level of mutual, statistical dependence between two variables [27]. In the context of theoretically predicted and experimentally measured cross-sections, let's consider two variables: X (theoretically predicted cross-sections) and Y (experimentally measured cross-sections). The Pearson's correlation coefficient can be used to determine how closely these two variables are related. Typically their values range from −1 to +1. When we interpret the value of r:

- If r = +1, it indicates the strongest positive linear relationship between X and Y. This means that Y also increases consistently as X increases.
- If r = -1, it indicates the strongest negative linear relationship between X and Y. This means that as X increases, Y decreases consistently.
- If r = 0, it indicates no linear relationship between X and Y. In other words, there is no consistent pattern in how they vary.

The present study offers a correlation between the theoretically predicted and experimentally measured production cross-section of medically important radionuclides, ^{68}Ga and ^{64}Cu, produced from the interaction of α-projectile with a ^{66}Zn target at α-energies ranging from ≈ 10 - 40 MeV. The quantitative values for the association were obtained using the statistical Pearson's correlation coefficient, or R. The correlation between theoretical predictions and experimental measurements of production cross-sections is measured by Pearson's correlation coefficient or R. This correlation primarily focuses on the trend of the association for the production of medically important radionuclides at the maximum regions of the two cross-sections [45, 46]. The mathematical description is given by:

$$R = \frac{\Sigma_{i=1}^{N} (X_{Ti} - \langle X_T \rangle (X_{Ei} - \langle X_{Ei} \rangle)}{N-1 (S_{XT})(SX_E)} \quad (3.26)$$

Where

$$\langle X_T \rangle = \frac{1}{N} \Sigma_i^N (X_{Ti}) \quad (3.27)$$

$$S_{XT} = \sqrt{\frac{1}{N-1} \Sigma_{i=1}^{N} (X_{Ti} - < X_T >)} \quad (3.28)$$

$$< X_E >= \frac{1}{N} \Sigma_{i}^{N} (X_{Ei}) \quad (3.29)$$

$$S_{XE} = \sqrt{\frac{1}{N-1} \Sigma_{i=1}^{N} (X_{Ei} - < X_E >)} \quad (3.30)$$

Where R is the correlation coefficient and unit less, ⟨XT⟩ and ⟨XE⟩ are the mean theoretical and experimental reaction cross-sections, respectively, and X_{Ti} and X_{Ei} are the theoretical and experimental total cross-sections of i^{th} the value, respectively. N is the number of the theoretical and experimental data, and S_{XT} and S_{XE} are the standard deviations of the total theoretical and experimental cross-sections, respectively [47]. If $0 \leq R \leq 0.3$, the correlation is weak and positive, $0.3 \leq R \leq 0.7$ describes a moderate correlation, and $0.7 \leq R \leq 1$, the correlation is strong.

3.7. Thick Target Yield calculations

The yield calculation for medically important radionuclides is an important aspect of nuclear medicine and radiopharmaceutical production. Yield refers to the amount of a specific radionuclide that is produced during a nuclear reaction or irradiation process. The calculation of yield is essential for determining the efficiency and effectiveness of a production process and ensuring that the desired amount of radionuclide is obtained for medical use. The cross-section of ^{68}Ga and ^{64}Cu radionuclides and its impurities employed in the thick target yield calculation were obtained from Talys1.95 (G) code.

One must consider the relevant nuclear reactions and their respective cross-sections to calculate the thick target yield of medically important radionuclides like ^{68}Ga and ^{64}Cu. For example, the most common production route ^{68}Ga involves the reaction ^{66}Zn(α, x)^{68}Ga, where alpha particles irradiate with ^{66}Zn nuclei, producing ^{68}Ga along with other reaction products. The cross-section of this reaction, which represents the probability of the reaction occurring at a given energy, is crucial for yield estimation. Experimental data on cross-sections are often available from nuclear reaction databases or EXFOR [48]. The thick target yield for the production of ^{68}Ga and ^{64}Cu via the investigated reaction channel has been calculated using equation (2.73)

CHAPTER FOUR

RESULT AND DISCUSSIONS

In this study, the yield of medically important ^{68}Ga and ^{64}Cu radionuclides and their impurities were investigated at ≈ 10 - 40 MeV α-energy through the interaction of α-projectile with a ^{66}Zn target. The statistical reaction-model codes TALYS1.95 (G), EMPIRE3.2, and COMPLET predictions were utilized to compare and analyze experimentally measured production cross-section in the EXFOR data [48].

In the COMPLET code, the level density parameter a is determined using the formula a = A/K MeV, where A is the nucleon number of a compound system, and K is an adjustable constant that can be changed to better fit the experimental data [3]. This level density parameter significantly impacts the equilibrium state components of a cross-section. As can be seen from figure 4.1(a) to fit the experimental data, K (K = 8, 10, and 12) values were varied for ^{66}Zn (α, x)^{68}Ga reaction channel produced in the interaction of α + ^{66}Zn system. It may be observed from this figure that up to ≈ 35 MeV in the region where maximum production cross-section is attained, COMPLET code overestimate and, above this point, underestimate the experimentally measured production cross-sections. It may further be observed from Figure 4.1(a) that a value of K=12, in general, better reproduced the experimentally measured values. For the same ^{66}Zn (α, x)^{68}Ga reaction, another sensitive input parameter called initial exciton number (n_o), which denotes the initial configuration of particles and holes, was also varied to n_o = 4, 5, and 6 to fit the measured cross section. As shown in Figure 4.1 (b), the prediction of COMPLET code for n_o = 4 better reproduced the measured cross section. Furthermore, the mean free path multiplier (MFM), another sensitive input parameter in the COMPLET code, is also varied (MFM=1, 2, and 2.5) to fit the experimentally measured cross section for the same reaction channel. As shown in Figure 4.1(c), a value of MFM=2.5 better reproduced the experimentally measured values. Thus, in COMPLETE code predictions, K=12, n_o=4, and MFM= 2.5 were used.

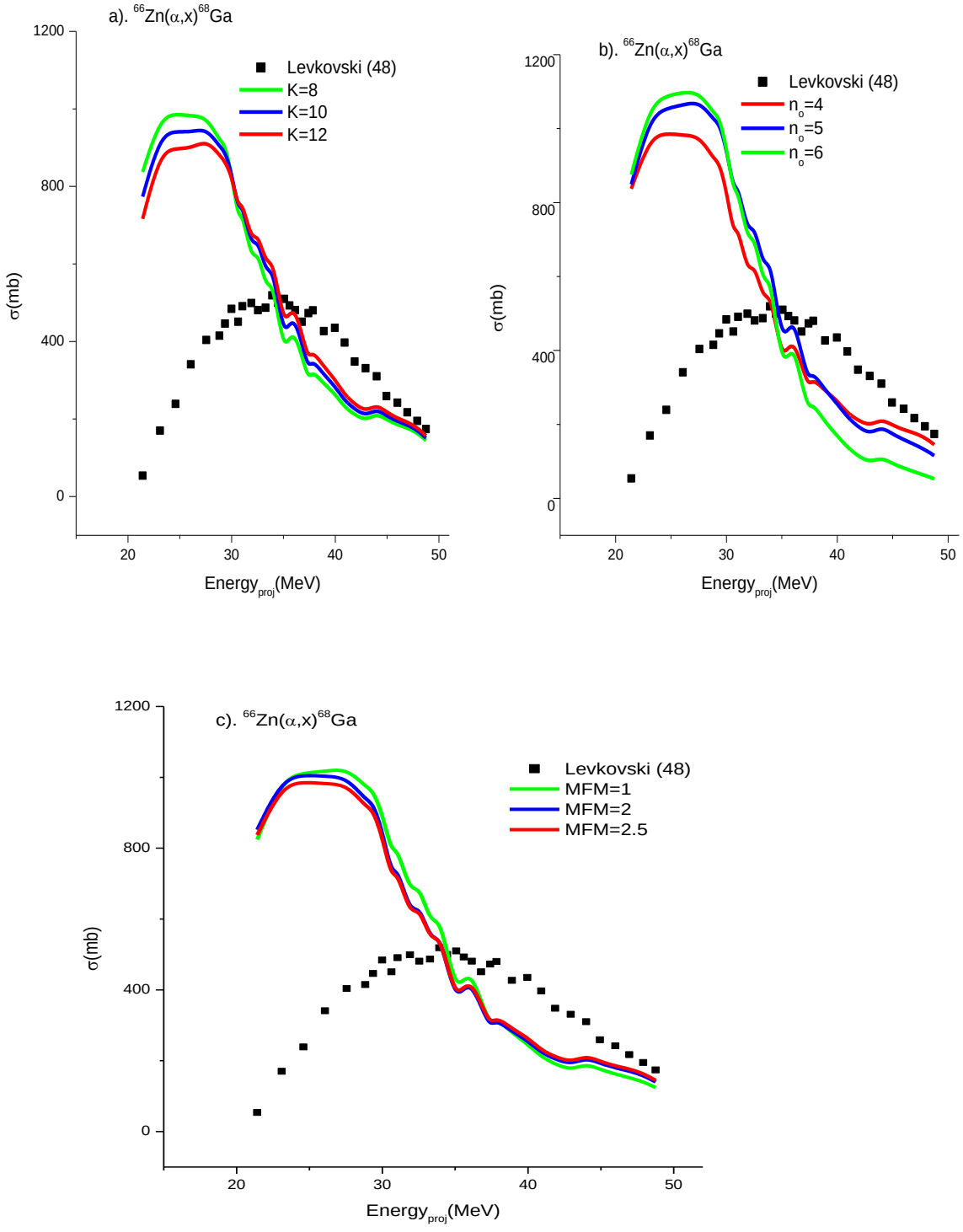

Figure.4.1. Experimentally measured and theoretically predicted cross section of ^{68}Ga.

In the production cross-section investigations, TALYS1.95 (G) and EMPIRE3.2 codes provide options to select different level density models from the respective codes. In this work, we chose the Enhanced Generalized Superfluid Model for the EMPIRE 3.2 code and the Exciton model with optical model transition rates for the TALYS1.95 (G) code. These level density models from the respective computer codes were selected because these models have successfully predicted production cross-sections.

4.1. Production of ^{68}Ga Radionuclide

The medically important ^{68}Ga radionuclide can significantly be produced from the interaction of α-projectile with ^{66}Zn-target at ≈10 - 40 MeV. The ^{68}Ga radionuclide has a half-life of ($T_{1/2}$ = 67.7 min) and decays through positron emission (β^+ = 88.88%) and electron capture (ε = 11.11%). ^{68}Ga radionuclide, is used for the labeling of ligands targeted to specific protein expression products such as receptors, enzymes, and antigens; small effector or hapten molecules for pre-targeted imaging; and various compounds for imaging of general biologic properties and processes such as proliferation, apoptosis, hypoxia, glycolysis, and angiogenesis [49]. In addition, it can be used to investigate thrombosis and atherosclerosis and detect pancreatic cancer, myocardial perfusion, pulmonary perfusion, and ventilation. Figure 4.2 displayed the experimentally measured production cross-section along with theoretical predictions for ^{68}Ga radionuclide produced via (α, x) channel in the interaction of α-projectile with ^{66}Zn target at ≈10-40 MeV.

It may be observed from Figure 4.2 that the predicted production cross sections using TALYS 1.95(G) and EMPIRE3.2 codes, in general, reproduced satisfactorily to the experimental measurements of Levkovski [48]. It is worth mentioning that higher energy regions TALYS1.95 (G) better predicted the measured cross-sections. It may further be seen from Figure 4.2 that up to ≈ 35 MeV, where the maximum cross-section is attained, COMPLETE code overestimates measurements of Levkovski [48]. The maximum production cross-section value for ^{68}Ga radionuclide produced via the (α, x) channel obtained using the TALYS1.95(G) code is about ≈ 637.8 mb at ≈ 30.6 MeV. From Table.2, Pearson's correlation coefficient value R ≈ 0.84 for TALYS1.95 (G) confirms a strong positive correlation between theoretically predicted and experimentally measured production cross-sections.

However, R ≈ 0.06 for the COMPLET code represents a weak positive relationship, and 0.66 for EMPIRE3.2 confirms a moderate positive correlation relationship, respectively, between theoretically predicted and experimentally measured production cross-sections.

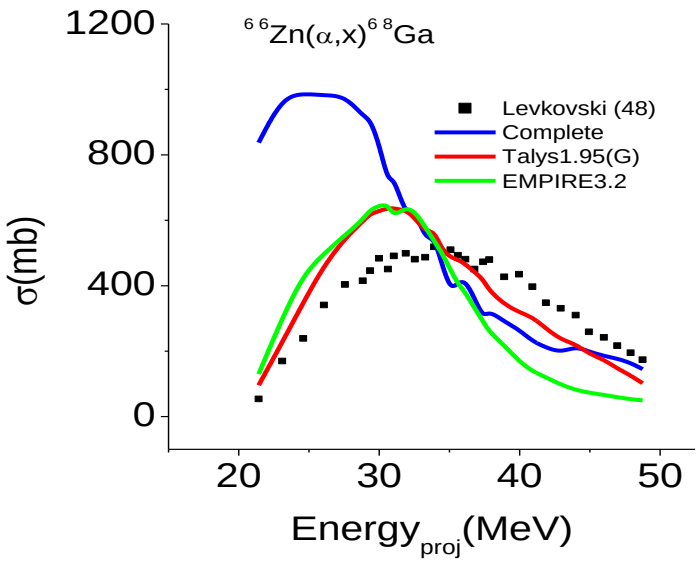

Figure.4.2. Experimentally measured and theoretically predicted cross section of ^{68}Ga.

4.1.1. Contribution of isotopic impurities in ^{68}Ga production

To calculate the thick target yield and produce a medically important radionuclide, cross-section data of competing reactions that may produce radioactive impurities must be considered in addition to the desired reaction. Therefore, in addition to the cross-section of the desired radionuclide, one must consider competing nuclear reactions that could result in isotopic impurities. In irradiations of ^{66}Zn isotopes with alpha projectiles, besides ^{68}Ga radionuclide, other isotopic radionuclides, such as ^{67}Ga and ^{66}Ga, are produced. Thus, the primary concern regarding the radioisotopic purity of ^{68}Ga is related to isotopic impurities, which are difficult to separate using chemical processes. In this study, the TALYS1.95 (G) code, which satisfactorily predicted the production of ^{68}Ga, was utilized to predict cross sections of isotopic impurities produced during the reaction α-projectile with ^{66}Zn-target at ≈10 - 40 MeV.

According to TALYS1.95 (G) calculations, the potential radionuclides of Ga that are produced as impurities along with ^{68}Ga are ^{67}Ga and ^{66}Ga. ^{67}Ga radionuclide has half-life ($T_{1/2}$ =3.26 days) and decays through electron capture (ε = 100%). ^{66}Ga is another radioisotopic impurities produced through the ^{66}Zn(α,x)^{66}Ga reaction. ^{66}Ga radionuclide with half-life ($T_{1/2}$: 9.49 h) decays through positron emission (β^+ = 56%) and electron capture (ε = 44%). Figure 4.3 shows the theoretically calculated cross sections of ^{68}Ga radionuclide and its impurities ^{66}Ga and ^{67}Ga produced during the interaction as a function of alpha particle energies. From figure 4.3, in the energy window between ≈ 20 MeV to ≈ 28 MeV, where maximum production of ^{68}Ga is attained, the only significant product is ^{68}Ga, and no considerable impurities are present. As we increase from ≈ 28 MeV, the contribution of production of ^{68}Ga will start decreasing, and the production of ^{67}Ga will increase, which increases impurity during production of ^{68}Ga. The impurities can be avoided by setting the energy window below ≈ 28 MeV, where maximum production of ^{68}Ga radionuclide can be achieved in the interaction of α-projectile with ^{66}Zn-target via (α, x) reaction channel.

Table 1: Q values and threshold energies for investigated ^{68}Ga, ^{67}Ga, and ^{66}Ga radionuclides.

Nuclear reaction	Q-Value (MeV)	Threshold energy (MeV)
^{66}Zn(α, x)^{68}Ga	-12.5	13.3
^{66}Zn(α, x)^{67}Ga	-14.5	15.4
^{66}Zn(α, x)^{66}Ga	-25.7	27.3

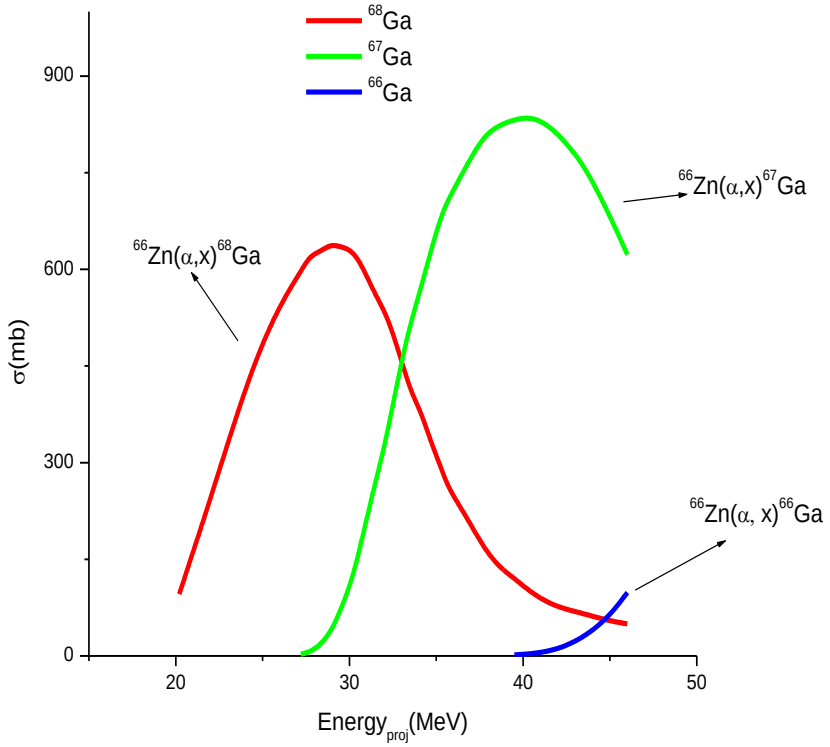

Figure.4.3. Calculated cross sections of radioisotope impurities of gallium produced in alpha-induced reaction on ^{66}Zn using TALYS 1.95(G).

4.2. Production of ^{64}Cu Radionuclide

The ^{64}Cu radionuclide, with a half-life ($T_{1/2}$=12.7 h), has an extensive application in radiotherapy and positron-emitting-tomography (PET) imaging to scrutinize several cancer-specific receptors, including the epidermal growth factor receptor and for treating colorectal cancer [50]. It decays in three modes: electron emission (β^- = 38.4%), electron capture (ε = 43.8%), and positron emission (β^+ =17.8%) [51]. Figure 4.4 displayed the experimentally measured and theoretically predicted cross sections of the medically important ^{64}Cu radionuclide produced in the interaction of α-projectile with ^{66}Zn target via the complex (α, x) channel. As can be seen from Figure 4.4, the predicted values using the TALYS1.95 (G) code agree with the experimental cross-section values measured by Nagame [52]. On the other hand, the predictions of COMPLET codes overestimate the measured production cross-sections of Nagame [52].

The maximum production cross-sections of ^{64}Cu radionuclide obtained using the TALYS 1.95(G) code is about ≈ 11.88 mb at ≈ 40 MeV. In addition, Table 2 shows Pearson's correlation coefficient value (R ≈ 0.82 for COMPLET, R ≈ 0.98 for TALYS1.95(G), and R ≈ 0.94 for EMPIRE3.2), which confirms a strong positive correlation between theoretically predicted and experimentally measured production cross-sections.

Table.2: Pearson's correlation coefficient, R, between experimental measured and theoretical predicted values of Levkovski [48] and Nagame [52]. R values represent the correlation between COMPLETE code (EMPIRE3.2 code), [TALYS1.95 (G)], and experimental values.

Radionuclide	COMPLETE code (EMPIRE3.2 code) [TALYS1.95 (G)]	
	Levkovski [48]	Nagame [52]
^{68}Ga	0.06 (0.66) [0.84]	-
^{64}Cu	-	0.82 (0.94) [0.98]

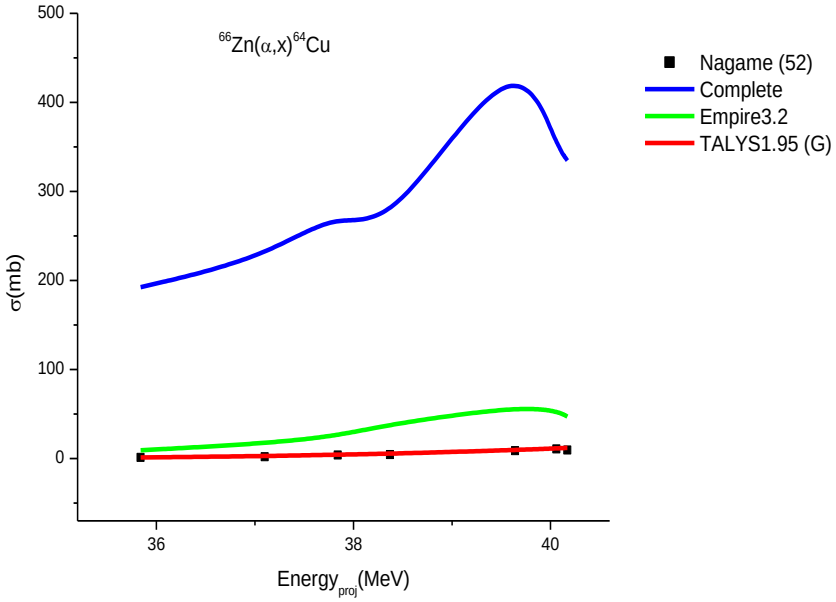

Figure.4.4. Experimentally measured and theoretically predicted excitation functions of ^{64}Cu.

4.2.1. Contribution of isotopic impurities in ^{64}Cu production

Similarly, in the production of medically important ^{64}Cu radionuclide, isotopic impurities could also be generated during the bombardment of α-projectile on ^{66}Zn-target. TALYS1.95 (G) code prediction suggested two significant ^{66}Cu and ^{62}Cu isotopic impurities populated via (α, x) reaction channel. Figure 4.5 displayed TALYS1.95 (G) predicted production cross sections of ^{64}Cu radionuclide along with its isotopic impurities ^{66}Cu and ^{62}Cu produced during α-bombardment on ^{66}Zn target. It may be seen from Figure 4.5, up to ≈40 MeV energy, where maximum production of ^{64}Cu obtained, the contribution from ^{66}Cu (≈ 0.009 mb at ≈39 MeV) and ^{62}Cu (≈ 0.0002 mb at ≈40 MeV) impurities are negligible.

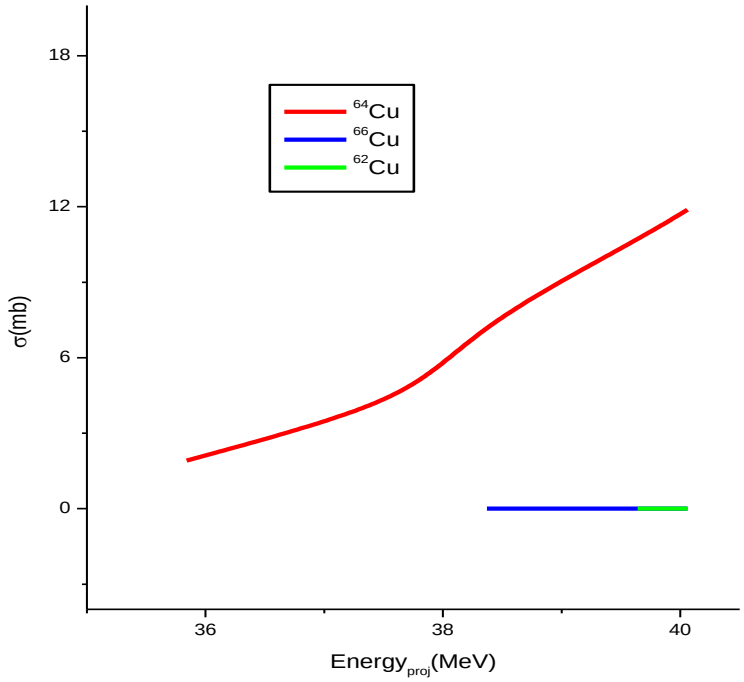

Figure.4.5. Calculated cross sections of radionuclide impurities of copper produced in alpha-induced reaction on ^{66}Zn using TALYS 1.95(G).

Table 3: Investigated nuclear reactions for the production of ^{64}Cu, ^{66}Cu, and ^{62}Cu with their Q values and threshold energies.

Nuclear reaction	Q-Value (MeV)	Threshold energy (MeV)
^{66}Zn(α, x)^{64}Cu	-16.6	17.6
^{66}Zn(α, x)^{66}Cu	-22.4	23.7
^{66}Zn(α, x)^{62}Cu	-29.1	30.9

4.3. Thick target yield

The thick target yield in the productions of medically important ^{68}Ga and ^{64}Cu radionuclides and the respective isotopic impurities produced in the interaction of α-projectile with ^{66}Zn-target were calculated using the formulation in equation (2.73).

4.3.1. Thick target yields of ^{68}Ga and its isotopic impurities ^{67}Ga, ^{66}Ga

The thick target yield for the production of ^{68}Ga radionuclide and its isotopic impurities populated in the interaction of α-projectile with a thick ^{66}Zn-target is calculated using the TALYS1.95 (G) predicted cross-sections and the yield formulation given by equation (2.73). The calculated thick target yield for ^{68}Ga radionuclide and its isotopic impurities ^{67}Ga and ^{66}Ga radionuclides produced via (α, x) reaction channel are shown in Figure 4.6. It may be seen from this figure that the production rate of ^{67}Ga increases from ≈ 28 MeV onwards, and the production of ^{66}Ga increases from ≈ 39 MeV. Given the energy region up to ≈ 28 MeV, where maximum ^{68}Ga production is attained, the contributions from its isotopic impurities are not significant. The maximum cross-section obtained in this region is ≈ 607.6 mb at ≈ 28 MeV. Thus, the thick target yield for medically important ^{68}Ga radionuclide is ≈ 39.6 GBq/μAh at ≈ 28 MeV with no significant contribution from its isotopic impurities ^{67}Ga and ^{66}Ga. Furthermore, it may be observed from Figure 4.6 that above ≈ 28 MeV, the yield of ^{67}Ga impurity begins contributing higher (≈ 41.3 GBq/μAh). However, this impurity can be eliminated using α-projectile energy of less than ≈ 29 MeV.

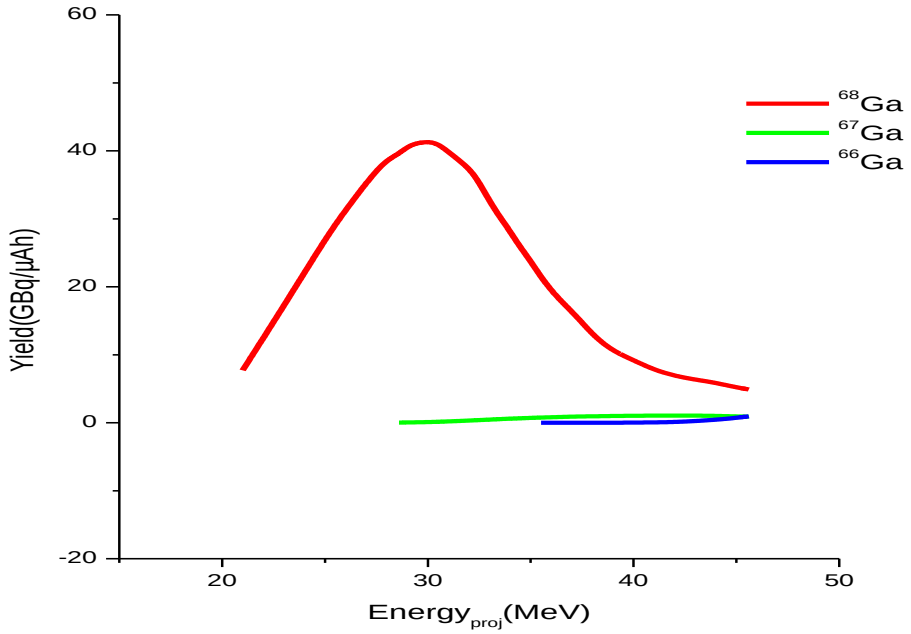

Figure.4.6. Calculated thick target yields for the $^{66}Zn(\alpha,x)^{68}Ga$, $^{66}Zn(\alpha,x)^{67}Ga$ and $^{66}Zn(\alpha,x)^{66}Ga$ reactions.

Table.4: Comparison of ^{68}Ga yields and predicted radioactive impurity yields for some selected alpha energies.

Isotope	possible nuclear reaction	half-life	Thick target yield (GBq/μAh)					
			21 MeV	25 MeV	28 MeV	32 MeV	37 MeV	41 MeV
^{68}Ga	$^{66}Zn(\alpha, x)^{68}Ga$	67.7 min	7.72	28.4	39.6	33.7	15.8	7.79
^{67}Ga	$^{66}Zn(\alpha, x)^{67}Ga$	3.26 days	0	0	0.02	0.44	0.91	1.06
^{66}Ga	$^{66}Zn(\alpha, x)^{66}Ga$	9.46 hours	0	0	0	0	0	0.11

Based on the data in Table 4, all impurities' combined thick target yield is much lower than the desired ^{68}Ga radionuclide. It can also be seen that no thick target impurity will be produced below 28 MeV alpha energy is used to produce ^{68}Ga.

4.3.2. Thick target yields of ^{64}Cu and its isotopic impurities ^{66}Cu, ^{62}Cu

Similarly, the calculated thick target yields of ^{64}Cu radionuclide and its isotopic impurities ^{66}Cu and ^{62}Cu produced in the interaction of α-projectile with ^{66}Zn are shown in Figure 4.7. As can be seen from this figure, the calculated thick target yield for ^{64}Cu is about 85.9 MBq/μAh at ≈40 MeV, at the point where the TALYS1.95 (G) predicted production cross section is maximum. Furthermore, the calculated thick target yields for the isotopic impurities ^{66}Cu and ^{62}Cu are negligible, with values of approximately 0.8 MBq/μAh for ^{66}Cu at ≈ 39 MeV and 0.1 MBq/μAh for ^{62}Cu at ≈ 40 MeV. This is due to the small production cross-sections of ≈ 0.009 mb at ≈ 39 MeV for ^{66}Cu and ≈ 0.0002 mb at ≈ 40 MeV for ^{62}Cu. Our calculated thick target yield of ^{64}Cu in the suggested energy region is 85.9 MBq/μAh at 40 MeV.

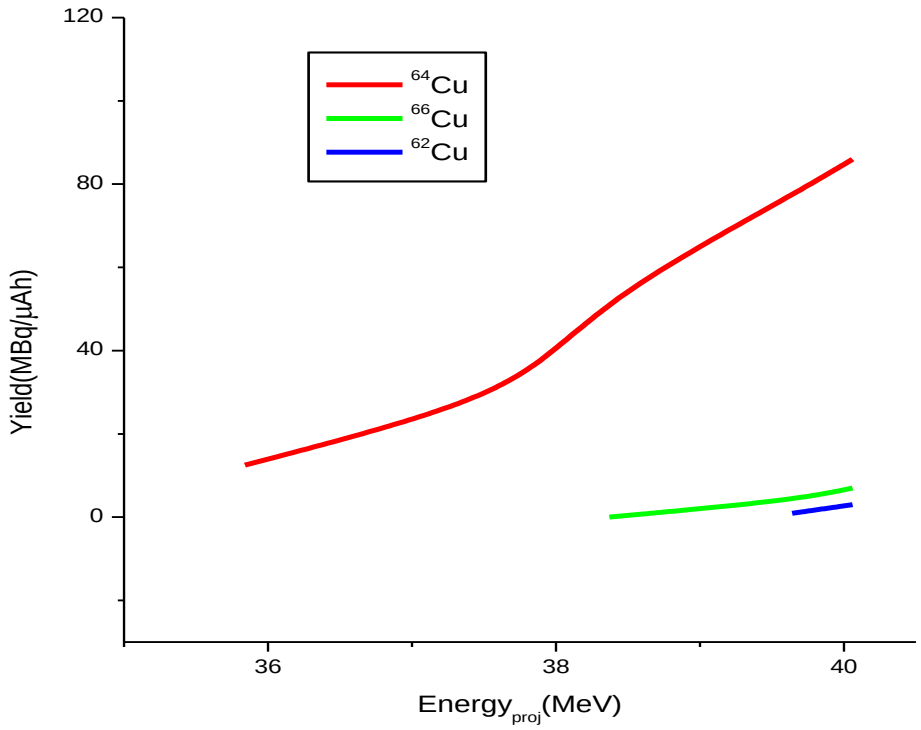

Figure.4.7.Calculated thick target yields for the ^{66}Zn(α,x)^{64}Cu, ^{66}Zn(α,x)^{66}Cu and ^{66}Zn(α,x)^{62}Cu reactions.

Table 5: Comparison of ^{64}Cu yields and predicted radioactive impurity yields for some selected alpha energies.

Isotope	possible nuclear reaction	half-life	Thick target yield (MBq/μAh)			
			35 MeV	37 MeV	39 MeV	40 MeV
^{64}Cu	$^{66}Zn(\alpha, x)\,^{64}Cu$	12.7 hour	12.5	34	77.3	85.9
^{66}Cu	$^{66}Zn(\alpha, x)\,^{66}Cu$	5.15 min	0	0	0.8	3
^{62}Cu	$^{66}Zn(\alpha, x)^{62}Cu$	9.74 min	0	0	0	0.1

From Table 5, the two impurities ^{66}Cu produced from $^{66}Zn(\alpha, x)\,^{66}Cu$ and ^{62}Cu produced from $^{66}Zn(\alpha, x)\,^{62}Cu$ nuclear reactions have negligible yield value; this is due to the very low nuclear cross-sections of the impurities in the given energy interval.

CHAPTER FIVE

SUMMARY AND CONCLUSION

The thick target yields for the productions of medically important ^{68}Ga and ^{64}Cu radionuclides populated in the interaction of α-projectile with ^{66}Zn-target were calculated at ≈10-40 MeV. The available data sets of experimental cross-sections taken from the EXFOR database were compared with the theoretical model calculations using nuclear reaction model codes COMPLETE, TALYS1.95 (G), and EMPIRE3.2. A good agreement was achieved for the measured data and calculated excitation functions using TALYS1.95 (G). The thick target yield of ^{68}Ga and ^{64}Cu has been deduced using the prediction of TALYS-1.95(G) production cross sections. The calculated thick target for ^{68}Ga radionuclide using the TALYS-1.95(G) predicted production cross-sections showed that ^{66}Zn(α, x)^{68}Ga reaction resulted in a maximum yield of up to ≈ 39.6 GBq/μAh at ≈ 28 MeV. In addition, calculating thick target yield for medically important ^{64}Cu radionuclide populated via ^{66}Zn(α, x)^{64}Cu reaction resulted in a maximum of 85.9 MBq/μAh at ≈ 40 MeV. Furthermore, the study indicated that the contribution coming from isotopic impurities is negligible.

REFERENCES

[1]. Auerbach, N., & Talmi, I. (1965). Energy levels, configuration mixing and proton neutron interaction in the Zr region. Nuclear Physics, 64(3), 458-480.

[2]. Cohen, S., Lawson, R. D., Macfarlane, M. H., & Soga, M. (1964). The effective interaction and identical-nucleon seniority for nuclei near Zr90. Physics Letters, 10(2), 195-198.

[3]. Asres, Y. H., Mathuthu, M., & Birhane, M. D. (2018). Analysis of reaction cross-section production in neutron induced fission reactions on uranium isotope using computer code COMPLET. Applied Radiation and Isotopes, 139, 81-85.

[4]. Aytekin, H., Baldık, R., & Alıcı, H. (2012). On the nuclear properties of ^{32}S, ^{64}Zn, ^{67}Zn, ^{89}Y, ^{90}Zr and ^{153}Eu targets used for production of ^{32}P, ^{64}Cu, ^{67}Cu, ^{89}Sr, ^{90}Y and ^{153}Sm therapeutic radionuclides. Annals of Nuclear Energy, 46, 128-133.

[5]. Nayak, D., & Lahiri, S. (1999). Application of radioisotopes in the field of nuclear medicine: I. Lanthanide series elements. Journal of radioanalytical and nuclear chemistry, 242(2), 423-432.

[6]. Takács, S., Aikawa, M., Haba, H., Komori, Y., Ditrói, F., Szűcs, Z. & Ukon, N. (2020). Cross sections of alpha-particle induced reactions on ^{nat}Ni: production of ^{67}Cu. Nuclear Instruments and Methods in Physics Research Section B: Beam Interactions with Materials and Atoms, 479, 125-136

[7]. Skakun, Y., & Qaim, S. M. (2008). Measurement of excitation functions of hellion-induced reactions on enriched Ru targets for production of medically important ^{103}Pd and ^{101m}Rh and some other radionuclides. Applied radiation and isotopes, 66(5), 653-667

[8]. AC07607271, A. (Ed.). (2009). Cyclotron produced radionuclides-physical characteristics and production methods. Internat. Atomic Energy Agency.

[9]. Artun, O. (2018). Calculation of productions of medical ^{201}Pb, ^{198}Au, ^{186}Re, ^{111}Ag, ^{103}Pd, ^{90}Y, ^{89}Sr, ^{77}Kr, ^{77}As, ^{67}Cu, ^{64}Cu, ^{47}Sc and ^{32}P nuclei used in cancer therapy via

phenomenological and microscopic level density models. Applied Radiation and Isotopes, 144, 64-79.

[10]. Aslam, M. T., Ali, W., & Hussain, M. (2021). Nuclear model analysis of the ^{65}Cu (α, n) ^{68}Ga reaction for the production of ^{68}Ga up to 40 MeV. Applied Radiation and Isotopes, 170, 109590.

[11]. Kambali, I., & Wibowo, F. A. (2023, May). Optimum radioactivity yield of Zirconium-89 radionuclide applicable for radioimmuno-PET imaging. In Journal of Physics: Conference Series (Vol. 2498, No. 1, p. 012010). IOP Publishing.

[12]. Amjed, N., Naz, A., Wajid, A. M., Hussain, M., & Qaim, S. M. (2023). Evaluation of cross section data for the low and medium energy cyclotron production of the non-standard positron emitting radionuclide ^{90}Nb. Radiation Physics and Chemistry, 209, 110996.

[13]. Neuhoff, J. (2021, April). DOE Isotope Program. R&D and Production of Isotopes for Space Applications. In Nuclear and Emerging Technologies for Space Conference.

[14]. Alemu, M. (2020). Study of proton induced reaction on rhodium isotope at various projectile energy (Doctoral dissertation, Mekdes Alemu).

[15]. Issa, S. A. A. M. (2009). Cross Section for Residual Nuclide Production by Proton–Induced Reaction with Heavy Target Elements at Medium Energies. PhD thesis.

[16]. Shehata, M. M. M. (2011). Radiochemical studies relevant to cyclotron production of the radionuclides $^{71, 72}$ As, $^{68\ Ge/68}$ Ga and $^{76, 77, 80m}$ Br.

[17]. Krane, K. S. (1991). Introductory nuclear physics. John Wiley & Sons.

[18]. Bertulani, C. A., & De Conti, C. (2010). Pauli blocking and medium effects in nucleon knockout reactions. Physical Review C, 81(6), 064603.

[19]. Aubrecht, G. (2003).A teacher's guide to the nuclear science wall chart. Contemporary Physics Education Project.

[20]. Taddesse, A. (2007).The Study Of α-Particle Induced Reaction on Gallium Isotopes (Doctoral dissertation, Addis Ababa University).

[21]. Kaplan, A., Aydin, A., Tel, E., & Şarer, B. (2009). Equilibrium and pre-equilibrium emissions in proton-induced reactions on 203,205 Tl. Pramana, 72, 343-353

[22]. Nigussie, B. (2012). Complete and incomplete fusion studies in some ^{14}N+ ^{59}Co systems (Doctoral dissertation, Addis Ababa University).

[23]. Blann, M. (1975). Preequilibrium decay. Annual Review of Nuclear Science, 25(1), 123-166.

[24]. Blann, M. (1971). Hybrid model for pre-equilibrium decay in nuclear reactions. Physical Review Letters, 27(6), 337..

[25]. Blann, M., & Vonach, H. K. (1983). Global test of modified pre compound decay models. Physical Review C, 28(4), 1475.

[26]. Mohsena, B. M. A. M. (2011). light charged particles induced nuclear reaction on some medium weight nuclei for particles applications.

[27]. Baak, M., Koopman, R., Snoek, H., & Klous, S. (2020).A new correlation coefficient between categorical, ordinal and interval variables with Pearson characteristics,Computational Statistics & Data Analysis, 152, 107043.

[28]. Tesfahun Markos (2014). complete and incomplete fusion studies in some ^{16}O +^{165}Ho systems at various energies.

[29]. Mengoni, A., & Nakajima, Y. (1994). Fermi-gas model parametrization of nuclear level density. Journal of Nuclear Science and Technology, 31(2), 151-162.

[30]. Konobeyev, A. Y., Fischer, U., Koning, A. J., Pereslavtsev, P. E., & Blann, M. (2011). Implementation of the geometry dependent hybrid model in TALYS. J. Korean Phys. Soc, 59, 935.

[31]. Capote, R., Herman, M., Obložinský, P., Young, P. G., Goriely, S., Belgya, T., ... & Talou, P. (2009). RIPL–reference input parameter library for calculation of nuclear reactions and nuclear data evaluations. Nuclear Data Sheets, 110(12), 3107-3214.

[32]. Baur, G., Bertulani, C. A., & Rebel, H. (1986). Coulomb dissociation as a source of information on radiative capture processes of astrophysical interest. Nuclear Physics A, 458(1), 188-204.

[33]. Olorunsola, A. B., Bamikole, J. A., Bello, A. A., & Ige, O. O. (2023). Theoretical prediction of neutron-induced radiative capture cross section on some isotopes of minor actinides from 10 keV-10 MeV. Journal of Nuclear and Radiation Sciences, 1, 1-11.

[34]. Qaim, S. M. (1982). Nuclear data relevant to cyclotron produced short-lived medical radioisotopes. Radiochim. Acta;(Germany, Federal Republic of), 30(3).

[35]. Dmitriev, P. P., Krasnov, N. N., & Molin, G. A. (1983).Yields of radioactive nuclides formed by bombardment of a thick target with 22-MeV deuterons (No. INDC (CCP)--210/L). International Atomic Energy Agency.

[36]. Qaim, S. M., Steyn, G. F., Spahn, I., Spellerberg, S., Van Der Walt, T. N., & Coenen, H. H. (2007). Yield and purity of ^{82}Sr produced via the ^{nat}Rb (p, xn) ^{82}Sr process. Applied radiation and isotopes, 65(2), 247-252.

[37]. Otuka, N., Dunaeva, S., Dupont, E., Schwerer, O., & Blokhin, A. (2011). The role of the nuclear reaction data centres in experimental nuclear data knowledge sharing. Journal of the Korean Physical Society, 59(2), 1292-1297.

[38]. Qaim, S. M. (2001). Nuclear data for medical applications: an overview. Radiochimica Acta, 89(4-5), 189-196

[39]. Noori, S., Akkurt, İ., & Demir, N. (2017). Comparison of excitation functions of longer and shorter lived radionuclides. Acta Physica Polonica *A*, *132*(3), 1186-1188.

[40]. Hauser, W., & Feshbach, H. (1952). The inelastic scattering of neutrons. Physical review, 87(2), 366.

[41]. Bauge, E., Delaroche, J. P., & Girod, M. (2001). Lane-consistent, semi-microscopic nucleon-nucleus optical model. Physical Review C, 63(2), 024607.

[42]. Herman, M., Capote, R., Sin, M., Trkov, A., Carlson, B. V., Oblozinsky, P., ... & Zerkin, V. (2013). EMPIRE3.2 Malta modular system for nuclear reaction calculations and nuclear data evaluation User's Manual (No. BNL-101378-2013). Brookhaven National Lab.(BNL), Upton, NY (United States). National Nuclear Data Center (NNDC).

[43]. Maritu Dagnaw(2017) Excitation Function Studies and Pre-Equilibrium Effect of Alpha Induced ^{93}Nb Reactions.

[44]. Hodgson, P. E. (1987), Compound nucleus reactions. Reports on Progress in Physics, 50(9), 1171.

[45]. Schober, P., Boer, C., & Schwarte, L. A. (2018). Correlation coefficients: appropriate use and interpretation. Anesthesia & analgesia, 126(5), 1763-1768.

[46]. Wang, J. (2012).On the relationship between Pearson correlation coefficient and Kendall's tau under bivariate homogeneous shock model. International Scholarly Research Notices, 2012.

[47]. Sedgwick, P. (2012). Pearson's correlation coefficient. Bmj, 345.

[48]. Levkovski, V. N. (1991). Cross sections of medium mass nuclide activation (A= 40-100) by medium energy protons and alpha-particles (E= 10 - 50 MeV). Inter-Vesi, Moscow, USSR.

[49]. Velikyan, I. (2011). Positron emitting [68Ga] Ga-based imaging agents: chemistry and diversity. Medicinal Chemistry, 7(5), 345-379.

[50]. Mou, L., Martini, P., Pupillo, G., Cieszykowska, I., Cutler, C. S., & Mikołajczak, R. (2022). ^{67}Cu production capabilities: A mini review. Molecules, 27(5), 1501.

[51]. Firestone, R. B. (1996). Table of isotopes, USA edited by VS Shirley.

[52]. Nagame, Y., Nakahara, H., & Furukawa, M. (1989). Excitation functions for α and 3He particles induced reactions on zinc. Radiochimica Acta, 46(1), 5-12.